The Whakamaru Magmatic System (Taupō Volcanic Zone, New Zealand), Part 1: Evidence from tephra deposits for the eruption of multiple magma types through time

Harmon, Lydia J, *ljharmo1@asu.edu, Department of Earth & Environmental Sciences, Vanderbilt University, 2301 Vanderbilt Place, Nashville, TN 37235, USA and School of Earth and Space Exploration, Arizona State University, 781 Terrace Mall, Tempe, AZ 85287, USA

Gualda, Guilherme A R, Department of Earth & Environmental Sciences, Vanderbilt University, 2301 Vanderbilt Place, Nashville, TN 37235, USA.

Gravley, Darren M, School of Earth and Environment, University of Canterbury, Private Bag 4800, Christchurch 8140, New Zealand.

Smithies, Sarah L, School of Earth and Environment, University of Canterbury, Private Bag 4800, Christchurch 8140, New Zealand.

Deering, Chad D, Michigan Tech University, Geological and Mining Engineering and Sciences, 1400 Townsend Drive, Houghton, MI 49931, USA.

ABSTRACT

The Whakamaru group eruptions (349 ± 4 ka; Downs *et al.*, 2014) are the largest known eruptions in the history of the young Taupō Volcanic Zone, Aotearoa New Zealand. The complex field relationships of the ignimbrites have thus far obscured the timing and history of their eruption(s). We present new evidence from fall deposits correlated with the Whakamaru eruptions to complement the ignimbrite record. Two coastal sections are characterized in detail. We group the tephra horizons into three packages: the older, smaller Tablelands and Paerata tephras; the overlying Kohioawa tephras (correlated with Whakamaru group eruptions); and the younger Murupara and Bonisch tephras. Major- and trace-element compositions suggest these tephras represent six distinct high-silica magma types, with the Kohioawa tephras representing three distinct magma compositions that are atypical of the TVZ. The distribution of Kohioawa magma types (types A, B, and C) changes through time, with the oldest deposits containing exclusively type A magma, the middle deposits containing types A and B, and the youngest deposits containing all three Kohioawa types. A combination of horizon-scale mineralogy and rhyolite-MELTS modeling suggests that only Kohioawa types B and C are saturated in sanidine – the presence of sanidine is atypical in Taupō Volcanic Zone magmas but has been previously documented in the Whakamaru group ignimbrites. Rhyolite-MELTS geobarometry reveals shallow storage pressures (~50-150 MPa) for Kohioawa magmas. At least three different melt-dominated magma bodies sourced the Kohioawa tephras – these magma bodies were laterally juxtaposed and co-erupted for most of the Whakamaru eruptions. Magmas that preceded and post-dated the Whakamaru eruptions have more typical TVZ compositions, emphasizing the unique features of the Whakamaru system.

KEY WORDS

Whakamaru group ignimbrites; Kohioawa tephras; Taupō Volcanic Zone; Geobarometry; Glass; Ignimbrite; Magma storage; Tephra

INTRODUCTION

Understanding large, caldera-forming eruptions requires understanding eruptive magma bodies through space and time. While there is substantial work focused on the pyroclastic flow deposits of large eruptions (i.e., ignimbrites), the co-erupted pyroclastic fall deposits (i.e., tephras) can preserve important information that may be obscured or not recorded by ignimbrites. For instance, the time-progression of eruptions may be poorly recorded in ignimbrites, but it is generally straightforward to interpret using the tephra record.

Constraining the distribution and storage conditions of melt-dominated magma bodies is critical to resolve how the crust can accommodate and erupt large volumes of magma (Charlier et al., 2007; Blundy and Cashman, 2008; Cashman and Giordano, 2014; Cooper and Kent, 2014; Wilson and Charlier, 2016; Gualda et al., 2018). For some magma systems, multiple melt-dominated magma bodies can erupt together (e.g., Cooper *et al.*, 2012; Gualda and Ghiorso, 2013; Bégué *et al.*, 2014a; Cashman and Giordano, 2014; Cooper, 2017; Swallow *et al.*, 2018; Gualda *et al.*, 2022), or a single, zoned magma body can erupt (e.g., Hildreth, 1979; Bachmann and Bergantz, 2004, 2008; Hildreth and Wilson, 2007; Deering *et al.*, 2011; Pamukçu *et al.*, 2013; Chamberlain *et al.*, 2015; Foley *et al.*, 2020). There is growing evidence suggesting that these melt-dominated magma bodies can be short-lived, lasting only centuries to a few millennia (Wilson and Charlier, 2009; Gualda *et al.*, 2012b; Cooper and Kent, 2014; Stelten *et al.*, 2014; Pamukçu *et al.*, 2015a; Gualda and Sutton, 2016; Allan *et al.*, 2017; Cooper *et al.*, 2017; Shamloo and Till, 2019); in contrast, the magma systems from which the melt-dominated magma is sourced can be active over timescales of tens to hundreds of thousands of years (Simon and Reid, 2005; Barboni *et al.*, 2015; Kaiser *et al.*, 2017; Reid and Vazquez, 2017).

We aim to reconstruct pre-eruptive storage conditions of magmatic systems. The main questions driving our research are:

1. How many melt-dominated magma bodies exist prior to large eruptions?
2. What are the pre-eruptive storage depths of the melt-dominated magma bodies?
3. How do the number and depths of the melt-dominated magma bodies change through the lifecycle of a large magma system?

To address these questions, we focus on the Whakamaru magma system, which produced large, ignimbrite-forming eruptions in the central Taupō Volcanic Zone (TVZ), Aotearoa New Zealand (Ewart, 1965; Martin, 1965; Ewart and Healy, 1966; Briggs, 1976a, 1976b; Wilson *et al.*, 1986, 2009; Houghton *et al.*, 1995; Brown *et al.*, 1998).

Previous work indicates that there are multiple magma types (Brown *et al.*, 1998), but it is as yet unclear how these relate to magma bodies. Deciphering how the melt-dominated magma bodies were organized in the crust and erupted through time is notoriously challenging for the Whakamaru magma system due to the complex field relationships and compositional signatures of the deposits (Brown *et al.*, 1998; Downs *et al.*, 2014).

The Whakamaru group ignimbrites are divided into five mappable units (Figure 1) (Grindley, 1960; Martin, 1961, 1965; Healy *et al.*, 1964; Ewart and Healy, 1966; Briggs, 1976a, 1976b; Leonard *et al.*, 2010; Downs *et al.*, 2014); however, it is not clear how the eruption(s) relate to the mapped units (Briggs, 1976a, 1976b; Wilson *et al.*, 1986; Brown *et al.*, 1998). Ar-Ar ages of the Whakamaru group ignimbrites are indistinguishable at 349 ± 4 ka, with the exception of the later erupted Paeroa Subgroup at 339 ± 5 ka (Downs *et al.*, 2014), and the ignimbrite deposits do not overlap sufficiently in the field to definitively determine relative timing of the eruption(s) (Wilson *et al.*, 1986; Brown *et al.*, 1998).

Tephra deposited as pyroclastic fall deposits offers an opportunity to remedy some of these issues (Bonadonna and Phillips, 2003; Folch and Felpeto, 2005; Brown *et al.*, 2012; Costa *et al.*, 2012; Matthews *et al.*, 2012b; Houghton and Carey, 2015, Bonadonna *et al.*, 2015), as they exhibit clear relative ages due to their sequential deposition.

In this work, we use detailed characterization of tephras from the Bay of Plenty (Aotearoa New Zealand), originally characterized by Manning (1995, 1996), to document in more detail the tephra packages that correlate with the Whakamaru group ignimbrites. We then use evidence from physical volcanology, glass compositions, and rhyolite-MELTS geobarometry (Gualda *et al.*, 2012a, Gualda and Ghiorso, 2014) to decipher how the melt-dominated magma bodies were organized in the crust, and how they erupted and changed through time.

Nomenclature

A note on nomenclature: After Smithies *et al.* (2023), we refer to ***magma*** as a geological material that includes melt (typically silicate in composition), but which can also include crystals and bubbles. A ***magma body*** is a parcel of magma that is in contact with rocks or other magmas, with clear boundaries. We can define melt-dominated magma bodies and magma mush bodies. A ***melt-dominated magma body*** is composed of crystal-poor magma that is readily eruptible and typically has a suspension of crystals and bubbles. A ***magma mush body*** is composed of crystal-rich magma that contains a framework of touching crystals, possibly with bubbles present. The magma mush is unlikely to be readily erupted. A ***magma type*** is a compositionally and texturally homogeneous group of magmas where a given magma type may be characteristic of a magma body, or it may be present in multiple magma bodies. The ***magma system*** includes all magma bodies through time.

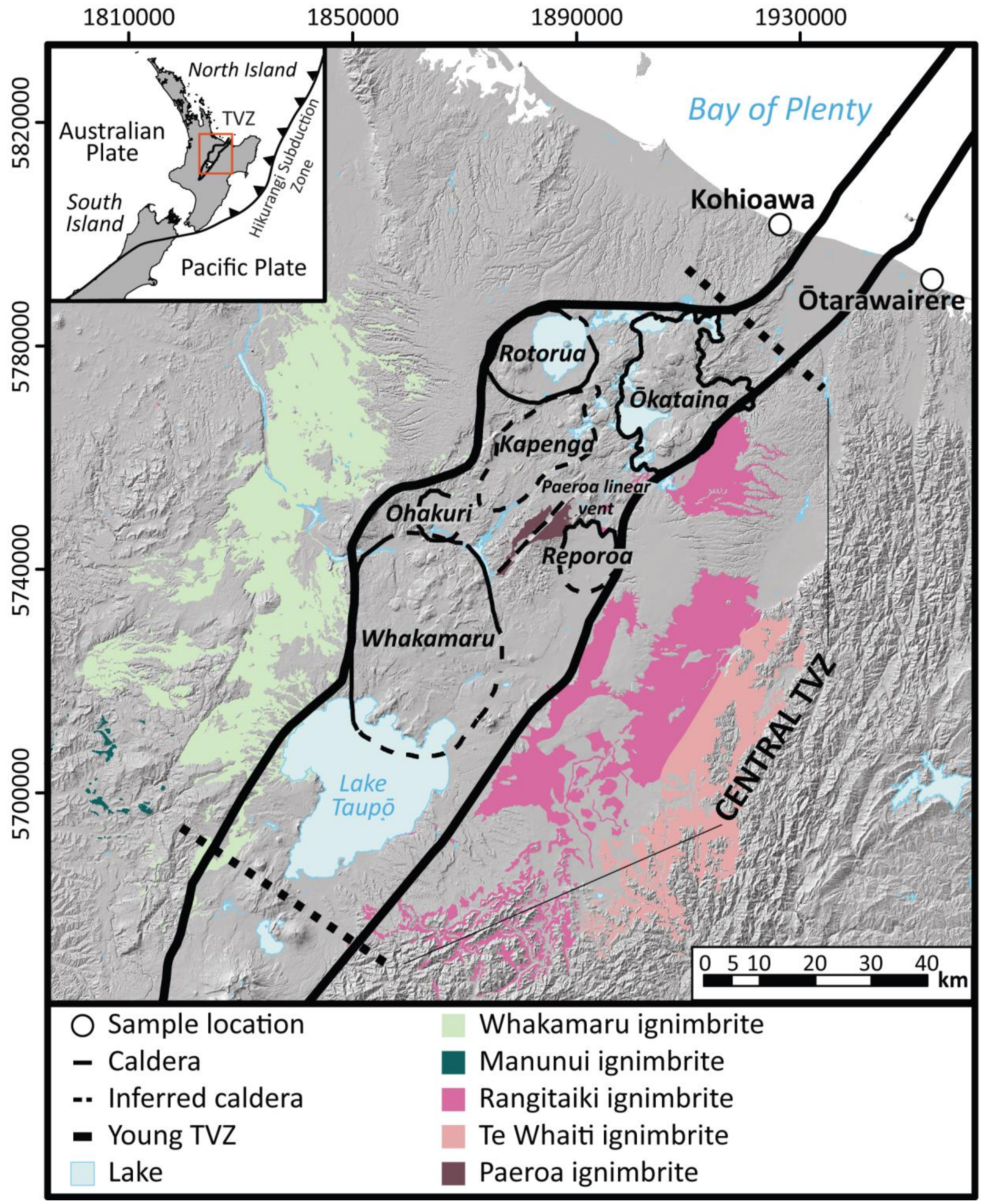

Figure 1 Map of the Taupō Volcanic Zone (TVZ), New Zealand. The outline of the young TVZ and major calderas of the most recent ignimbrite flare-up (~350-240 ka) are shown. The Whakamaru caldera is the southernmost and largest caldera. The

locations of the two coastal tephra sequences, the Kohioawa section (37°52'27.25"S, 176°42'40.85"E) and Ōtarawairere section (37°57'11.80"S, 177° 1'26.20"E), are marked with circles at the coast, ~90 km northeast of the caldera. Calderas are mapped after Leonard *et al*. (2010), outline of the young TVZ after Wilson et al. (1995), and the Whakamaru group ignimbrites are shown after Leonard *et al.* (2010), Brown *et al.* (1998), and Downs *et al.* (2014). Coordinate system is in meters in the New Zealand Transverse Mercator 2000 projected on the New Zealand Geodetic Datum 2000. The map inset shows the location of the TVZ within the North Island of New Zealand.

GEOLOGICAL BACKGROUND

The Taupō Volcanic Zone

The TVZ is a northeast-southwest rifted arc in the North Island of New Zealand (Figure 1) (Wilson *et al.*, 1995). The central TVZ is one of the most active silicic volcanic systems in the world (Houghton *et al.*, 1995; Wilson *et al.*, 1995), having produced at least 6000 km^3 of silicic magma over the last ~1.6 Ma (Wilson *et al.*, 2009), with silicic activity starting at ~1.9 Ma (Eastwood *et al.*, 2013; Chambefort *et al.*, 2014).

Over this time, there have been three ignimbrite flare-up periods in the TVZ, which were especially intense periods of ignimbrite-forming volcanism (Houghton *et al.*, 1995). The largest and most recent ignimbrite flare-up episode, from ~350 to ~240 ka (Houghton *et al.*, 1995; Gravley *et al.*, 2007, 2016; Wilson *et al.*, 2009), erupted >3000 km^3 of magma from at least six calderas in the central TVZ (see Figure 1; Gravley et al., 2016, and references therein). The Whakamaru group eruptions mark the beginning of this episode, after which at least six additional large (50-150 km^3 dense rock equivalent, DRE), caldera-forming eruptions occurred (Houghton *et al.*, 1995; Wilson *et al.*, 2009; Leonard *et al.*, 2010; Gravley *et al.*, 2016). The compositional, textural, and mineralogical distinctions between the Whakamaru magmas and the magmas that fed the later flare-up eruptions imply potential differences in source and evolution of the magmas through time (Deering *et al.*, 2010; Gravley *et al.*, 2016; Gualda *et al.*, 2018, Smithies *et al.*, 2023).

Whakamaru group eruptions and their deposits

The Whakamaru group ignimbrites have most recently been Ar-Ar dated to 349 ± 4 ka, with the smaller Paeroa Subgroup ignimbrites (with a volume estimate on the order of 110 km^3) having slightly younger ages of 339 ± 5 ka (Downs *et al.*, 2014). The Whakamaru magma system had a complex history of magma generation (Saunders *et al.*, 2010) and of erupting multiple, distinct magma types (Brown *et al.*, 1998), potentially during one main eruption phase (with the exception of the younger Paeroa Subgroup) (Brown *et al.*, 1998; Downs *et al.*, 2014) or over multiple eruptive phases (Grindley, 1960; Martin, 1961; Wilson *et al.*, 1986; Houghton *et al.*, 1995). Zircon ages from the Whakamaru group eruptions show that there was an active magma system ~50-100 ka prior to eruption (Matthews, 2011), with older zircon ages implying that it was active up to ~250 ka prior to eruption (Brown and Fletcher, 1999), indicating a long history of maturation. Evidence from plagioclase and quartz show much shorter timescales (<300 a) for the final assembly, homogenization, and eruption (Saunders *et al.*, 2010; Matthews *et al.*, 2012a), which imply relatively short timescales for the ephemeral melt-dominated magma bodies consistent with what is seen elsewhere (Druitt *et al.*, 2012; Gualda *et al.*, 2012b; Pamukçu *et al.*, 2015b, 2020; Gualda and Sutton, 2016; Allan *et al.*, 2013, 2017).

Four widespread mappable ignimbrite units are described – the Whakamaru, Manunui, Rangitaiki, and Te Whaiti ignimbrites (Grindley, 1960; Healy *et al.*, 1964; Ewart, 1965; Martin, 1965; Ewart and Healy, 1966; Briggs, 1976a, 1976b), with the Paeroa Subgroup documented as a group of three younger ignimbrites derived from the same magma system but likely erupted from a separate source (Houghton *et al.*, 1995; Wilson *et al.*, 2009; Leonard *et al.*, 2010; Downs *et al.*, 2014). The Whakamaru and Manunui ignimbrites are distributed to the west of the caldera, and the Rangitaiki and Te Whaiti ignimbrites are distributed to the east of the caldera (Figure 1). Wilson *et al.* (1986) propose that the Manunui and Te Whaiti ignimbrites could be correlative and erupted earlier, and that the Whakamaru and Rangitaiki ignimbrites could be correlative and erupted later. There is no documented significant time-break between the eruptions (Brown *et al.*, 1998; Downs *et al.*, 2014). In this work, we refer to the whole collection of ignimbrites as the Whakamaru group ignimbrites; Whakamaru ignimbrite refers to the specific ignimbrite *sensu stricto*.

Brown *et al.* (1998) reports four different compositional rhyolite pumice types (types A, B, C, D) from the erupted ignimbrites, with some ignimbrites containing multiple pumice types. The lack of overlap of the ignimbrites in the field and the presence of multiple pumice types in the ignimbrites begs the question of how the melt-dominated magma bodies were stored in the crust and erupted through time. Brown *et al.* (1998) calculate shallow Al-in-hornblende storage pressures (~ 100-150 MPa) and interpret that the least evolved and hottest material likely erupted first, with sanidine only present in the later erupted, more evolved material. The presence of sanidine in the latter units is corroborated by drill core and field data (Martin, 1961, 1965; Ewart, 1965; Ewart and Healy, 1966; Briggs, 1976a). The characteristics of the magma types as described by Brown *et al.* (1998) are given in the supplementary material.

The Rangitawa tephra (formerly the Mt. Curl tephra) has been suggested to be correlative with the Whakamaru group eruptions based on glass shard major-element compositions, ferromagnesian mineralogy, and similarity in paleomagnetic dates and zircon fission-track ages (Kohn *et al.*, 1992; Alloway *et al.*, 1993; Pillans *et al.*, 1996; Lowe *et al.*, 2001). The Rangitawa tephra is crystal-rich (Kohn *et al.*, 1992) and it is found across the North Island and as far away as the Chatham Islands (Holt *et al.*, 2010), as well as in offshore deposits (Matthews et al., 2012, and references therein). It has been interpreted to be related to a Plinian phase of the Whakamaru eruptions and is composed of type A magma (Brown *et al.*, 1998), which is predominant in the Whakamaru and Rangitaiki ignimbrites (Wilson *et al.*, 1986; Matthews *et al.*, 2012b). However, there is a caveat that fall deposits have never been documented in contact with the Whakamaru group ignimbrite sequence (Brown *et al.*, 1998). Therefore, these fall deposits can only be generally correlated with the Whakamaru group magma system via mineralogy and glass geochemistry.

Here, we compare Rangitawa tephra data (Matthews *et al.*, 2012b) and Whakamaru group ignimbrite data (Bégué *et al.*, 2014b; Gualda *et al.*, 2018) to the Kohioawa tephras (Manning, 1995, 1996) to investigate the correlation between Whakamaru magmas and the Kohioawa tephras and to elucidate their history and the pre-eruptive conditions of crystallization and storage.

Field relations and previous work

Manning (1995, 1996) correlates tephras across the eastern Bay of Plenty, including a sequence that he proposes to be correlative with the Whakamaru group eruptions, ~90 km northeast of the caldera (Manning, 1995, 1996) (Figures 1-2). We use the formal names proposed by Manning (1995, 1996) for the units within the tephra sequence, focusing specifically on the Tablelands B-D, Paerata, Kohioawa, and Murupara-Bonisch units. The Tablelands B-D tephras and Paerata tephra are interpreted to be derived from smaller eruptions, perhaps from the Ōkataina volcanic center (Manning, 1995). Importantly, there is a well-developed paleosol at the top of the Paerata tephras, indicating a substantial time break before the eruptions that formed the Kohioawa tephras (Figure 2). The Kohioawa tephras are substantially thicker than other units. Using glass compositions, Manning (1995) recognizes two distinct chemical populations of glass, with one of the Kohioawa tephra glass types being correlative with that recorded in the widespread Rangitawa tephra. Similarly, Manning (1996) states that one of the glass populations is similar to that in the Rangitaiki ignimbrite (type A of Brown *et al.,* 1998) but interprets the Kohioawa tephras to be from two coeval eruptions.

The Murupara-Bonisch tephras post-date the Kohioawa tephras and precede the Matahina ignimbrite-forming eruption (322 ± 7 ka; Leonard *et al.*, 2010), which is observed overlying these tephras at the Kohioawa section (Figure 2a) (Manning, 1995, 1996). Both the Murupara-Bonisch and the subsequent Matahina ignimbrite (Bailey and Carr, 1994) are interpreted to have erupted from the Ōkataina volcanic center (Manning, 1995, 1996). Full descriptions of the different units are provided in the supplementary material.

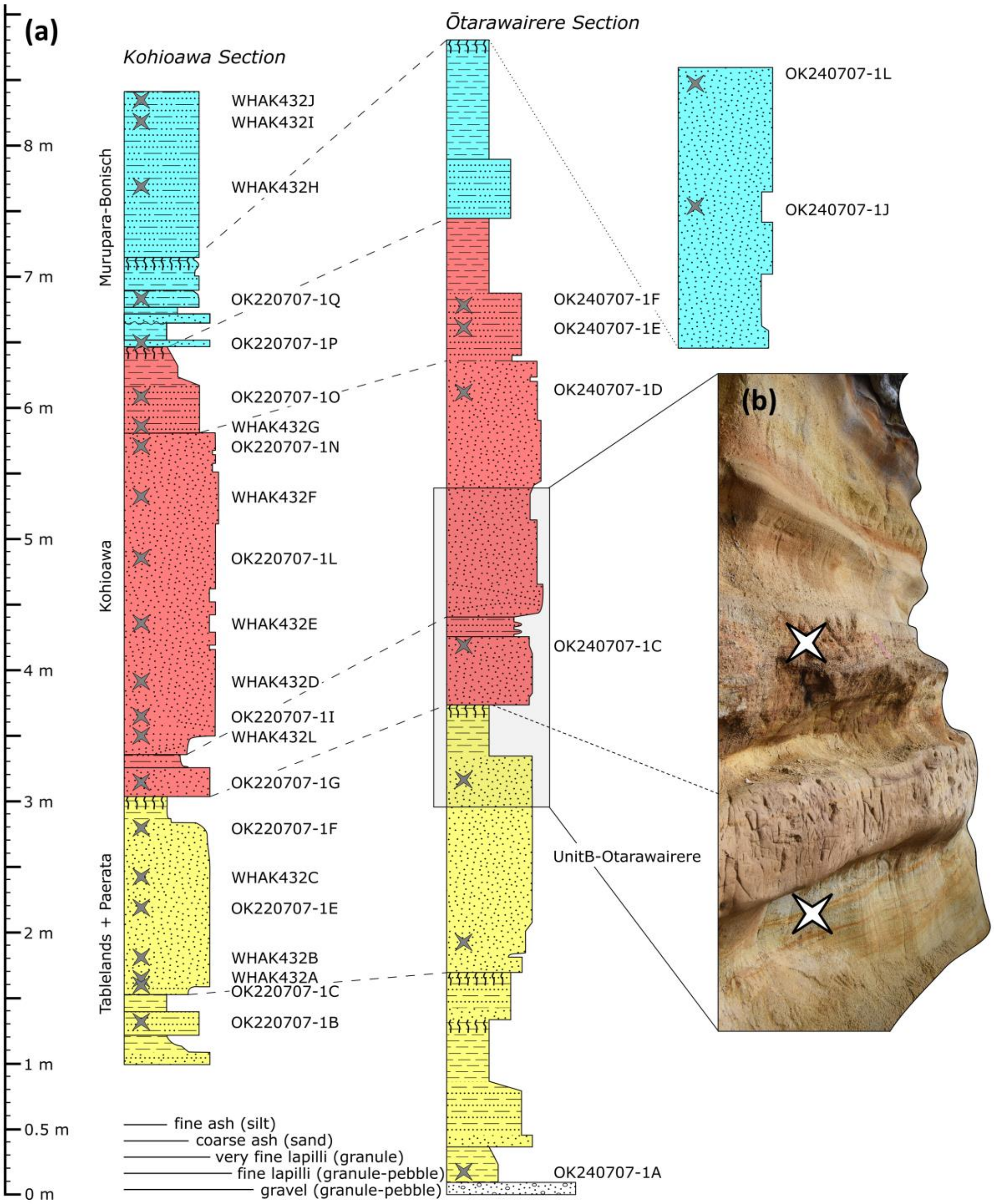

Figure 2 a) Schematic section of the two tephra sequences (Kohioawa and Ōtarawairere) studied in this work and b) a field photo of a portion of the Ōtarawairere tephra sequence. In a), the width of the units in the schematic corresponds to grain size. The patterns follow the Federal Geographic Data Committee Digital Cartographic Standard for Geologic Map Symbolization (FGDC-

STD-013-2006). The paleosols are denoted by vertical wiggly lines, which do not extend through entire packages to enhance readability and because the thicknesses of the paleosols often vary across an exposure. Measured thicknesses of paleosols are provided in the supplementary material. The 22 samples from Kohioawa section and 8 samples from Ōtarawairere section are marked with gray X's and labeled. The sample "UnitB-Ōtarawairere" in the Ōtarawairere section was sampled as a mixture of tephra from the top and bottom of this horizon, marked by X's. Correlations between units in the Kohioawa and Ōtarawairere sections are marked with dashed lines. The top of the Ōtarawairere section is shown at the top right of the figure, as indicated by the dotted line. The yellow basal units comprise the Tablelands and Paerata unit; the red middle unit is the Kohioawa unit; the top light-blue unit is the Murupara-Bonisch unit. The Kohioawa unit is subdivided into three subunits, as indicated by the dashed lines. A general description of the units is found in Table 1; a detailed description of each horizon is found in the supplementary material. b) The field photo shows a part of the Ōtarawairere section (from ~3 m to ~5.5 m, as indicated by the light gray box). This photo highlights the transition from the Paerata unit to the Kohioawa unit. These units are separated by a thick paleosol, the top of which is marked by a dotted line. Two of the sample locations are marked by X's where the lower X corresponds to sample UnitB-Ōtarawairere, and the upper X corresponds to sample OK240404-1C.

METHODS

Our work focuses on two locations: the Kohioawa section and the Ōtarawairere section (Figures 1-2) of Manning (1995). We use a combination of 1) field observations and sampling, 2) major- and trace-element compositions of glass in tephra clasts, 3) zircon saturation geothermometry (Watson and Harrison, 1983; Boehnke *et al.*, 2013), and 4) geobarometry via rhyolite-MELTS (Gualda and Ghiorso 2012a, 2015; Gualda *et al.*, 2014; Bégué *et al.*, 2014b; Pamukçu *et al.*, 2015b; Harmon *et al.*, 2018) to determine the changes in volcanological deposition through time, the number and compositions of melt-dominated magma bodies, and the storage conditions of the melt-dominated magma bodies. A total of 146 clasts were analyzed in this study for major- and trace-element glass compositions, with five to six of the largest, pristine juvenile clasts chosen from each horizon. Clasts generally consist of larger coarse-ash sized to fine-lapilli sized pumice clasts. Major-element compositions are obtained by SEM-EDS and trace-elements by LA-ICPMS using the same methods as Gualda *et al.* (2018), Foley *et al.* (2020), Pamukçu *et al.* (2020, 2021), Smithies *et al.* (2023), among others. Full descriptions of the methods are reported in the supplementary material.

RESULTS

Field observations

We focus on four units from Manning (1995): Tablelands B-D, Paerata, Kohioawa, and Murupara-Bonisch units. The boundaries between them are defined by paleosols or distinct changes in physical volcanological characteristics. At both locations, the deposits are characterized by laterally continuous, mostly horizontal layers that can be traced for tens of meters. The exposure is divided into horizons that range mostly from ~1 cm to ~20 cm, and the thickest three horizons at each location are >1 m thick. The horizons are composed of mostly clast-supported, fine-grained volcanic material that ranges from orange-yellow to light-yellow to gray in color. Generally, the grain size within a specific horizon is consistent, although grain size varies from clay/ash-sized to very coarse sand-sized over the different horizons within the exposures. The make-up of the material is predominantly juvenile volcanic pumice clasts, a variable amount of smaller volcanic lithics and loose crystals, and sometimes a sandy matrix that indicates post-depositional water interaction (Manning, 1995).

There are three loess paleosols described at the Kohioawa section and four loess paleosols described at the Ōtarawairere section (Manning, 1995) indicating distinct time breaks. At the Kohioawa section, the paleosols mark the boundaries between the Paerata and Kohioawa units, between the Kohioawa and Murupara-Bonisch units, and an internal boundary within the Murupara-Bonisch unit. At the Ōtarawairere section, there is a paleosol between Tablelands C and Tablelands D horizons and the thickest paleosol (~20-40 cm, although the thickness varies across the outcrops) marks the break between the Paerata and Kohioawa units. There is no discernible paleosol between Kohioawa and Murupara-Bonisch units at the Ōtarawairere section (Figure 2a).

A general description of each unit is provided in Table 1 and a schematic of the outcrops shown in Figure 2a. A detailed log of each horizon, including grain size, observed mineralogy, and paleosols is given in the supplementary material.

Mineralogy

Mineralogy of the tephra was described and recorded at the horizon scale through the sequence in the field and via optical microscopy. Plagioclase, quartz, hornblende, orthopyroxene, and Fe-Ti oxides are the main phases present in all horizons analyzed. Biotite is observed in the middle section. Results are summarized in the supplementary material. The felsic mineral componentry reveals that the first package of the Kohioawa unit is the only horizon in the Kohioawa unit that does not contain sanidine. We do not observe sanidine in the other units (Tablelands B and D, Paerata, and Murupara-Bonisch units).

Glass compositions

In most of the 146 clasts, the major-element analyses show that each clast has a single composition; however, there are 7 clasts for which a subdivision of glass analyses in two distinct populations was necessary. There is one additional clast for which we subdivided the glass into three different populations. There were no subdivisions of glass data for the Tablelands B and Tablelands D clasts, 2 subdivisions in the Paerata clasts (subdivisions for 5% of clasts), 1 subdivision in the Kohioawa clasts (subdivisions for 1% of clasts), and 4 subdivisions in the Murupara-Bonisch clasts (11% of the clasts). In all units, only a minority of clasts exhibit multiple glass compositions. All compositional data are reported as the mean and 1 standard deviation of individual clasts, with subdivisions denoted by "-A" or "-B" for the clasts with multiple populations.

We define six compositional groups using major- and trace-element compositions. The major-element compositions show that glasses in all clasts are high-silica rhyolites with 76.0-78.5 wt% SiO_2. Na_2O and K_2O are negatively correlated for all types, which could indicate some degree of Na-K exchange (Lipman, 1965; Scott, 1971; Pamukçu *et al.*, 2015b). The full data set of mean and standard deviation values of major and trace elements is reported in the supplementary material. The different geochemical characteristics of the Kohioawa glass compositional groups are defined and detailed in Table 2 and in Figures 3-5. The six compositional types are defined below.

Tablelands B, Tablelands D, and Paerata type

The first compositional type comprises glasses from the Tablelands B, Tablelands D, and Paerata clasts (labeled Tablelands + Paerata in Figures 3-5). This type is defined by relatively high CaO (>~1.0 wt%) and low K_2O (<~4.0 wt%) in major elements (Figure 3) and low Rb (110-140 ppm) and Cs (4-5 ppm) in the trace elements (Figure 4). These clasts have the highest Ba and the lowest light rare earth elements (LREE) abundances of all types.

Kohioawa types

The Kohioawa clasts exhibit three glass compositional types, which we call A, B, and C. Together, the Kohioawa types are the lowest in CaO and highest in K_2O of all glasses analyzed (Figure 3). Kohioawa types are higher in Rb, lower in Sr, and lower in Eu when compared to the other types (Figure 4).

Kohioawa type A can be distinguished clearly from types B and C by CaO and TiO_2, and by Mn, Sr, and Ba. It can be subtly distinguished by MgO and FeO, and by Cs, Zr, Eu, and Yb. There are no clear trends in SiO_2 and Al_2O_3. There are very subtle trends in many of the trace elements, but we highlight only those that have strong signatures. The rare earth element (REE) values can also distinguish type A from types B and C.

Types B and C are similar but can be subdivided on the basis of Ba contents. They can also be subdivided subtly in CaO and SiO_2, and by Sr, Eu, U, and Pb. Overall, both types are compositionally distinct from all other types in this study, with little to no overlap with the other types in trace-element compositions (e.g., Rb, Sr, Eu, Ba) (Figures 4-5). The quantitative trends to distinguish tephra types are provided in Table 2.

Kohioawa type A is the only type present in the lowest Kohioawa package. In the middle package, both Kohioawa types A and B are present. In the upper Kohioawa package, Kohioawa types A, B, and C are all present, although Kohioawa type C is the dominant glass type (Figures 6-7). There are 4 clasts that do not fall into any of the three Kohioawa groups. These are referred to as “undefined” and are not discussed further.

Murupara-Bonisch types

The Murupara-Bonisch clasts can be subdivided into two compositional types. The Murupara-Bonisch type A has lower SiO_2 and higher CaO (average ~1.2 wt%) and FeO (average ~1.4 wt%) than all other types (Figure 3). The Murupara-Bonisch type B overlaps with the Kohioawa type A for CaO (average 0.8 wt%) and SiO_2 (average 77.7 wt%) but differs in other elements (Figures 4-5). The Murupara-Bonisch type A is not present in the clasts from the first Murupara-Bonisch horizon, and it is the only type seen in the two uppermost Murupara-Bonisch horizons (Figures 6-7).

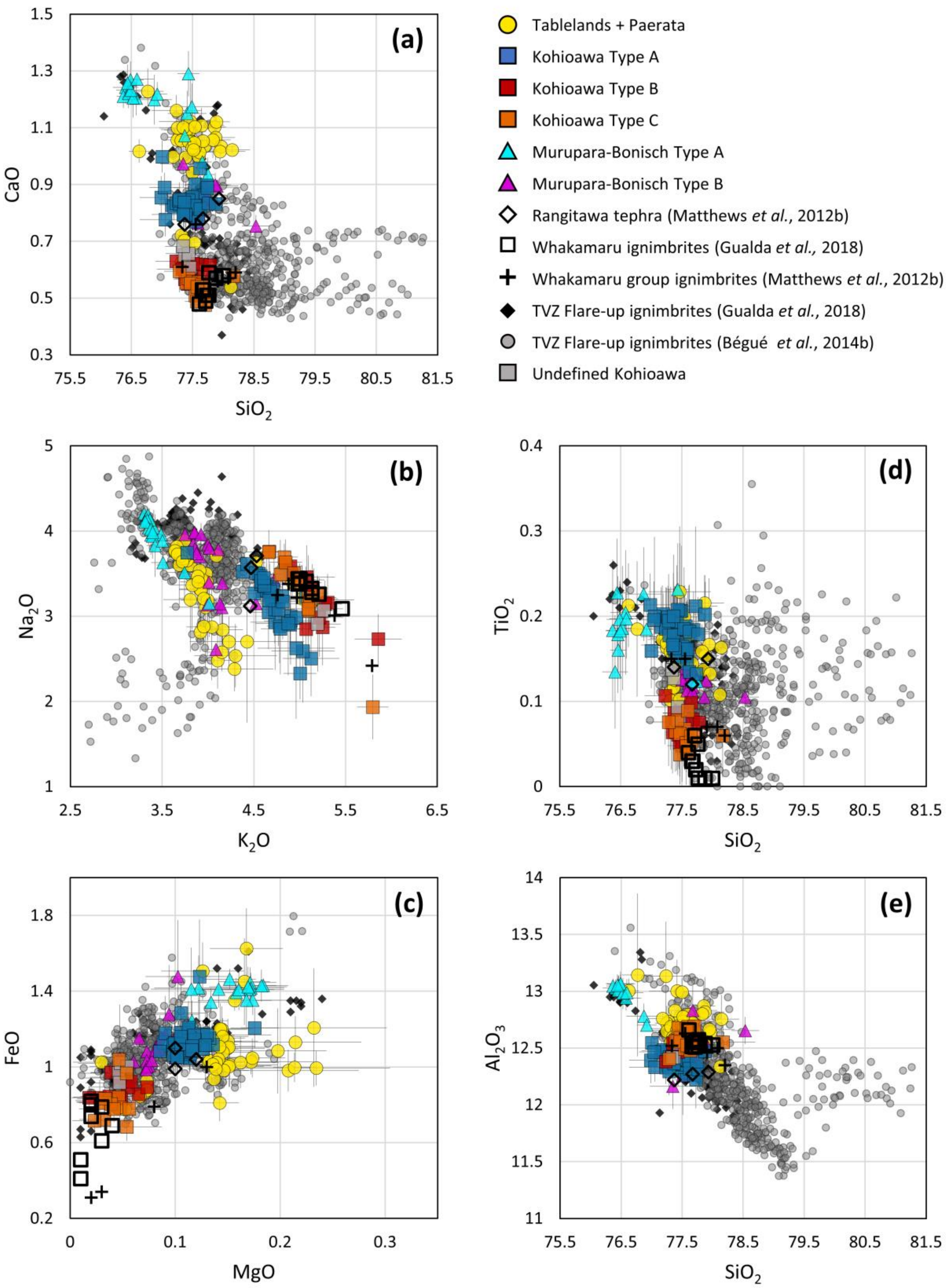

Figure 3 Major-element glass compositions of individual clasts from the Kohioawa and Ōtarawairere sections in a) CaO vs. SiO_2; b) Na_2O vs. K_2O; c) FeO vs MgO; d)

TiO_2 vs SiO_2; and e) Al_2O_3 vs SiO_2 space, reported as wt% of each oxide. There is one group for the Tablelands and Paerata unit represented by yellow circles; three groups for the Kohioawa unit represented by blue, red, and orange squares; and two groups for the Murupara-Bonisch unit represented by cyan and magenta triangles. Error bars (gray bars) are shown at the 1-sigma level for major- and trace-elements. We include literature data: 1) Rangitawa tephra data Matthews *et al.* (2012b), represented by open black diamonds; 2) Whakamaru ignimbrite data from Gualda *et al.* (2018), represented by open black squares, and from Matthews *et al.* (2012b), represented by black crosses; 3) ignimbrite data from the TVZ from other ignimbrite flare-up eruptions from Gualda *et al.* (2018), represented by black diamonds, and from Bégué *et al.* (2014b), represented by gray circles. In panels a and b, we exclude one composition from Bégué *et al.* (2014b,with 74.8 wt% SiO_2 and 0.65 wt% CaO) to improve readability. There are four “undefined” compositions from the Kohioawa tephras that do not fall into the three Kohioawa types, represented by gray squares.

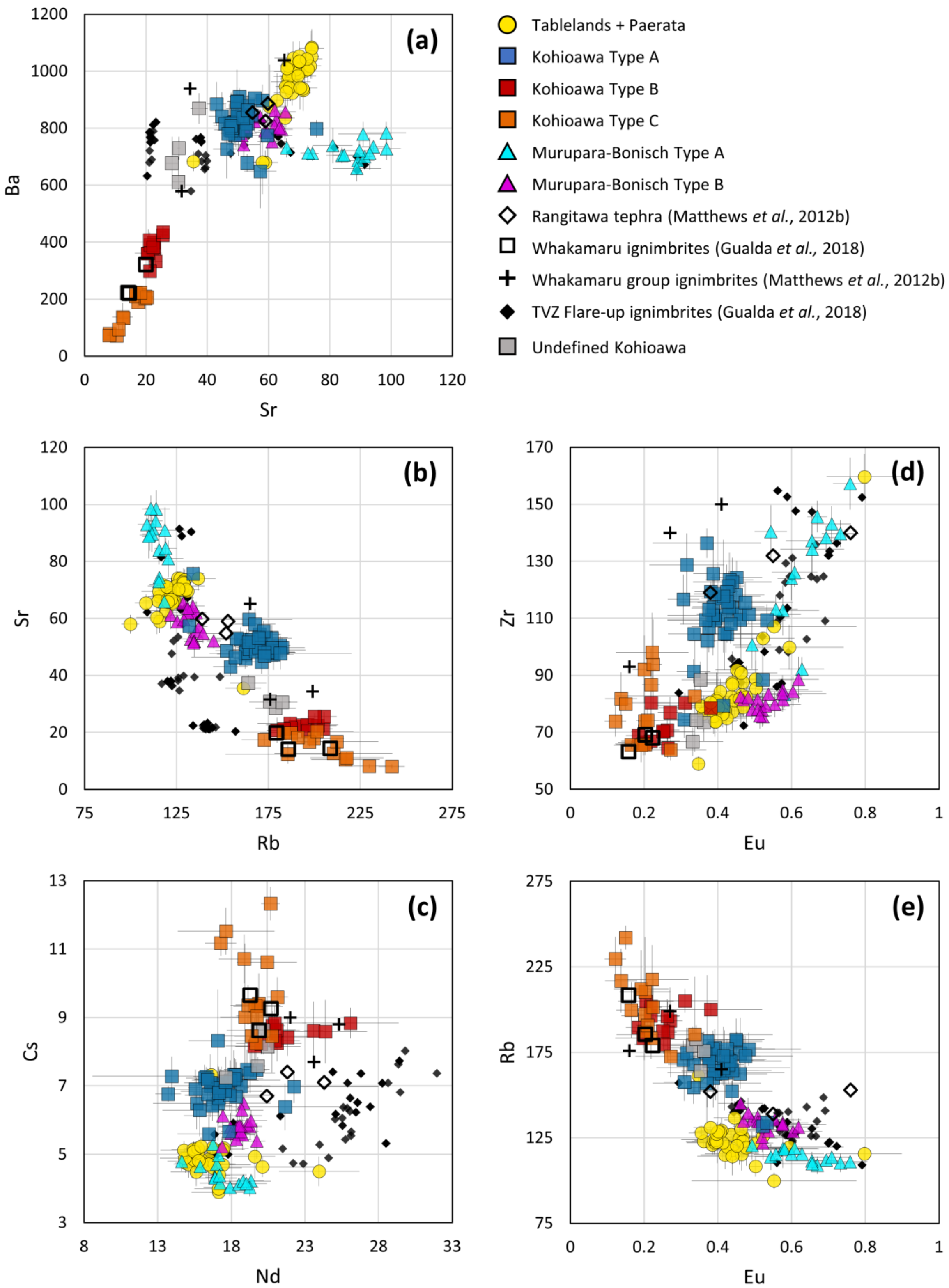

Figure 4 Trace-element compositions of glass from individual clasts of the Kohioawa and Ōtarawairere sections in a) Ba vs. Sr; b) Sr vs. Rb; c) Cs vs. Nd; d) Zr vs. Eu; and

e) Rb vs. Eu space reported in ppm. We include literature data: 1) Rangitawa tephra data from Matthews *et al.* (2012b); 2) Whakamaru ignimbrite data from Gualda *et al.* (2018), and from Matthews *et al.* (2012b); 3) ignimbrite data from the TVZ from other ignimbrite flare-up eruptions from Gualda *et al.* (2018). Error bars (gray bars) are shown at the 1-sigma level for major- and trace-elements. There are four undefined compositions from the Kohioawa tephras that do not fall into the three Kohioawa types, represented by gray squares. Different groups can be separated well using a combination of trace elements, particularly Ba and Sr.

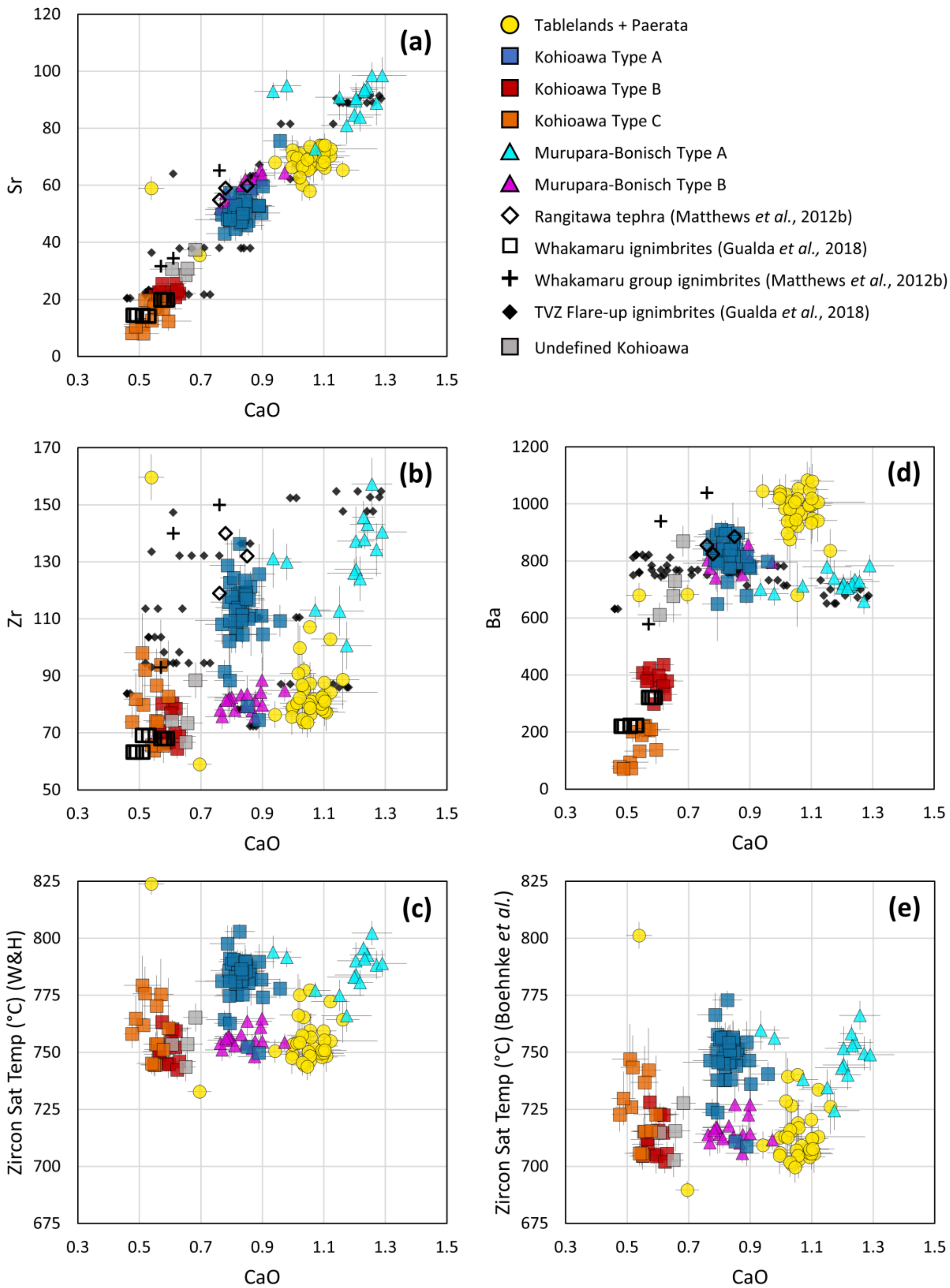

Figure 5 Select trace-element (ppm) and zircon-saturation temperatures (°C) vs. CaO (wt%) diagrams of glass from pumice clasts of the Kohioawa and Ōtarawairere

sections. Zircon-saturation temperatures are calculated using the Watson and Harrison (1983) calibration, labeled Zircon Sat Temp (W&H), panel c) and the Boehnke *et al*. (2013) calibration, labeled Zircon Sat Temp (Boehnke *et al.*), panel. e) Error bars (gray bars) are shown at the 1-sigma level for major- and trace-elements. The combination of CaO, Sr, and Ba leads to clear separation between the different compositional types identified in this work.. Zircon saturation temperatures are similar between populations, with Kohioawa type A and Murupara-Bonisch type A showing somewhat higher temperatures than the other units. Uncertainties for the average zircon saturation temperature per type are calculated as the standard deviation of zircon saturation temperatures for the given type. Average and one-sigma uncertainties are: 757 ± 15 °C for Tablelands B, Tablelands D, and Paerata (using the Watson and Harrison (1983) calibration; 716 ± 19 °C using the Boehnke *et al*. (2013) calibration); 782 ± 10 °C (746 ± 13 °C) for Kohioawa type A; 752 ± 7 °C (713 ± 9 °C) for Kohioawa type B; 760 ± 12 °C (724 ± 14 °C) for Kohioawa type C; 787 ± 12 °C (748 ± 11 °C) for Murupara-Bonisch type A; and 756 ± 4 °C (716 ± 6 °C) for Murupara-Bonisch type B

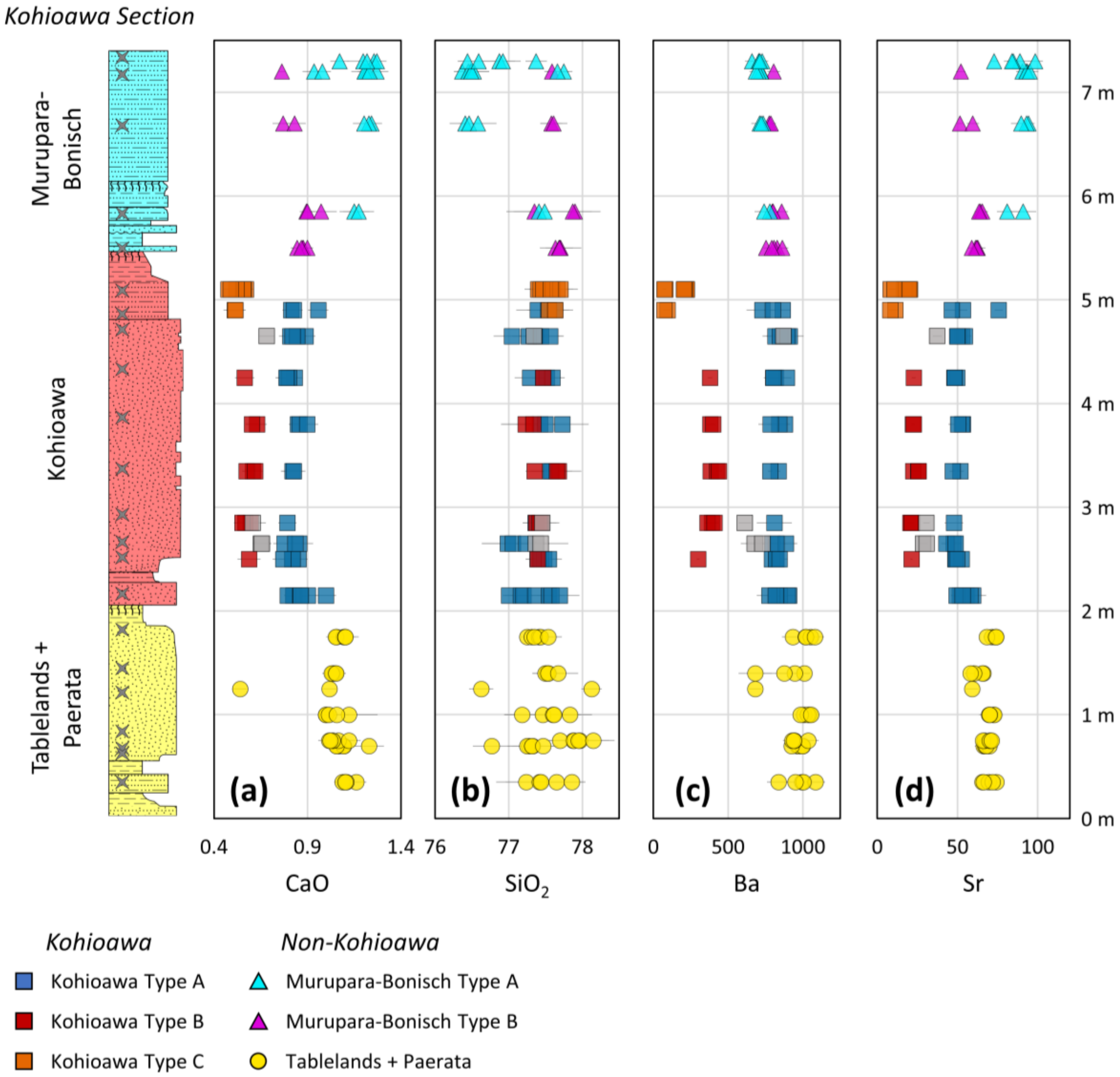

Figure 6 Major- and trace-element compositions of glass from individual clasts of the Kohioawa section as a function of height in the section. The yellow basal unit comprises the Tablelands and Paerata unit; the red middle unit is the Kohioawa unit; the top light-blue unit is the Murupara-Bonisch unit. Elements shown are a) CaO (wt%); b) SiO_2 (wt%); c) Ba (ppm); and d) Sr (ppm). Kohioawa type A is the only type present in the lower subunit of the Kohioawa unit; Kohioawa type C is the only type present in the upper subunit of the Kohioawa unit. Note the sharp compositional

transitions from Tablelands and Paerata to Kohioawa to Murupara-Bonisch units. The symbology is the same as in Figures 3-5.

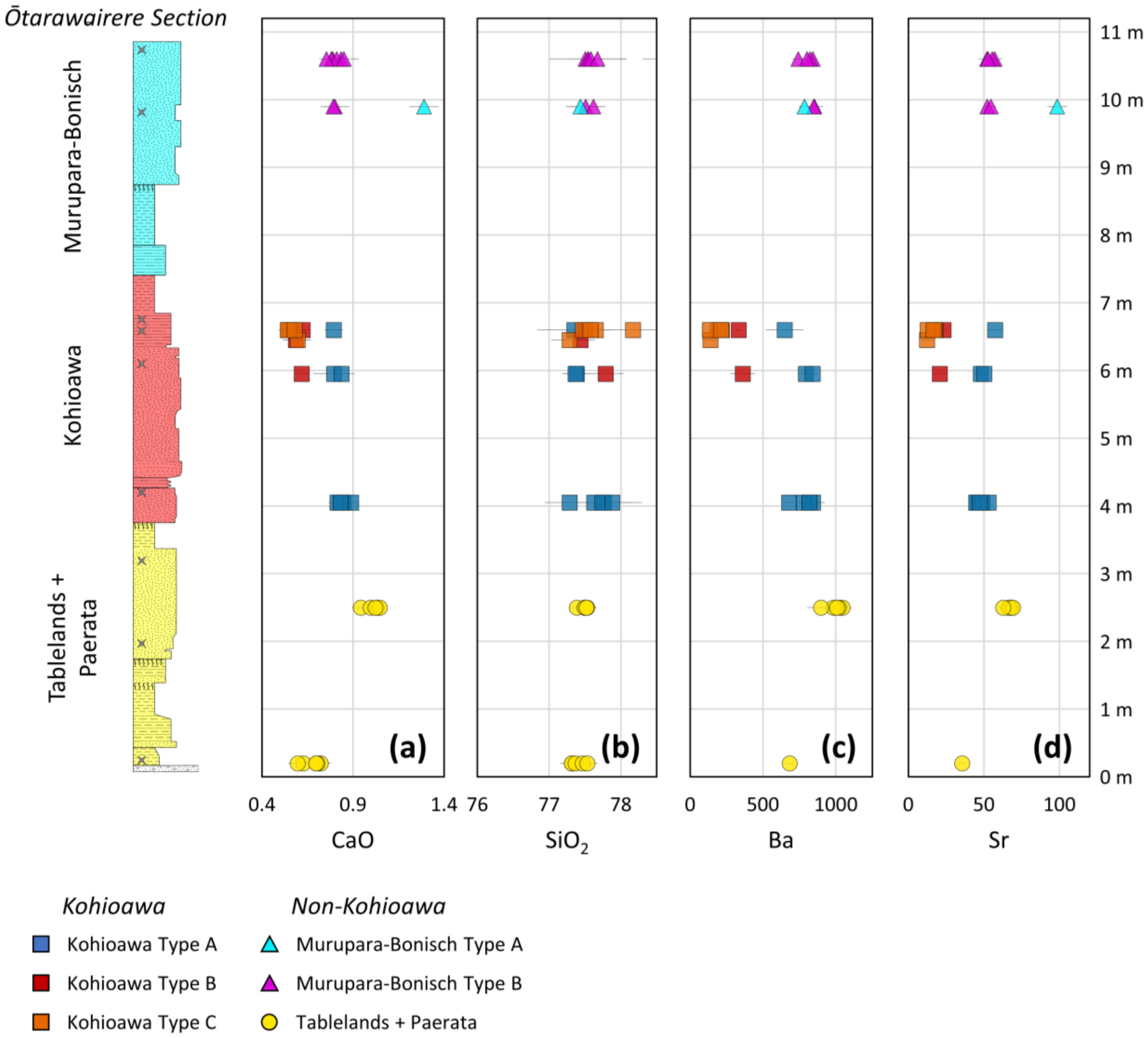

Figure 7 Major and trace-element compositions of glass from individual clasts of the Ōtarawairere section as a function of height in the section. The yellow basal unit comprises the Tablelands and Paerata unit; the red middle unit is the Kohioawa unit; the top light-blue unit is the Murupara-Bonisch unit. Elements shown are a) CaO (wt%); b) SiO_2 (wt%); c) Ba (ppm); and d) Sr (ppm). The number of samples from the Ōtarawairere section is much smaller than from the Kohioawa section, but the general

observations are consistent between the two sections with the exception that the uppermost sampled horizon in the Kohioawa unit shows Kohioawa types A, B, and C are present in this horizon. The symbology is the same as in Figures 3-5.

Geothermometry

We use zircon saturation geothermometry to determine pre-eruptive magma storage temperatures. All temperatures are reasonable estimates for rhyolitic magma stored in the upper crust. The temperatures calculated for Kohioawa type A are systematically higher than those calculated for Kohioawa types B and C. The lower temperatures of Kohioawa types B and C are very similar to both the Tablelands and Paerata type and the Murupara-Bonisch type B temperatures. The average and standard deviation of calculated temperature for each clast are included in the supplementary data.

Geobarometry

We use rhyolite-MELTS geobarometry to determine the storage conditions of the pre-eruptive magmas (Figures 8-9 and Figure 11, see discussion) (Gualda *et al.*, 2012a; Gualda and Ghiorso, 2014, 2015). This method determines the pressure at which melt (preserved as glass) is in equilibrium with the observed crystallizing mineral assemblage. We use the observed mineralogy in the horizons to constrain the phases potentially in equilibrium with the major-element glass composition. Quartz and plagioclase are ubiquitous in all units, suggesting equilibration between melt, plagioclase, and quartz.

As discussed above, the coarse ash-lapilli clasts are too small for us to unequivocally determine their mineral assemblages by direct observation, in particular the presence or absence of sanidine. We leverage the results of our rhyolite-MELTS pressure calculations to infer whether or not the glass composition is consistent with sanidine saturation in the individual clasts. We thus consider two potential assemblages:

1. quartz+plagioclase (qtz-1feld)
2. quartz+plagioclase+sanidine (qtz-2feld)

If a rhyolite-MELTS pressure calculation yields a qtz-2feld result, we conclude that such melt composition was very likely in equilibrium with sanidine. We emphasize that this does not affect the pressure calculation, given that – in this case – the qtz-1feld solution would be the same as the qtz-2feld pressure, with the advantage that qtz-2feld pressures have a smaller error than qtz-1feld pressure (see Gualda and Ghiorso, 2014). In Supplementary Figure 1, we show examples of calculations that yield qtz-1feld (no sanidine), qtz-2feld (sanidine-bearing), and no solution (glass composition does not record equilibrium between melt, quartz, and feldspars).

Of the 153 clast compositions, 121 compositions (79%) yield storage pressures (supplementary material). Individual pressure calculations are reported to the nearest 1 MPa (e.g., 122 MPa), and ranges of pressures are rounded to the nearest 5 MPa (e.g., 100-125 MPa).

All calculated storage pressures indicate upper crustal depths, with most values in the range of 50-255 MPa, with 90% of the calculations in the range of 70-235 MPa, and with clasts of each compositional type exhibiting a narrower range of pressures (Figures 8-9 and Figure 11, see discussion). Uncertainties estimated by Pitcher *et al.* (2021) show that the qtz-2feld pressures have a 1-sigma standard deviation of 24 MPa and the qtz-1feld pressures have a 1-sigma standard deviation of 38 MPa. Pamukçu *et al*. (2021) find 1-sigma standard deviations of ~10 MPa for qtz-1feld pressures from the Taupō ignimbrite. Uncertainties obtained via a Montecarlo error analysis on a glass composition from a pumice clast from the Whakamaru ignimbrite (whose composition was obtained using the same methods as this work) exhibit a qtz-2feld 1-sigma standard deviation of 13 MPa with several qtz-1feld results showing <22 MPa 1-sigma standard deviation (Smithies *et al.*, 2023). In all figures that contain geobarometry results, we plot the more conservative uncertainties of Pitcher *et al.* (2021).

Most clast compositions that produce a storage pressure yield results with the mineral assemblage qtz-1feld. With the exception of one Paerata clast (no sanidine observed in the horizon), the Kohioawa types B and C (all from sanidine-bearing horizons) are the only types to yield storage pressures with a qtz-2feld assemblage (19 compositions). The presence of the qtz-2feld assemblage indicates that these are the only compositional types with glass compositions consistent with sanidine saturation.

Some pressure trends through time become apparent (Figure 8). In particular, low storage pressures are consistent until the second horizon in the Murupara-Bonisch unit (in which higher storage pressures of ~200-275 MPa dominate). Also, several horizons exhibit clasts with low pressures (~50 MPa), particularly within the Kohioawa horizons.

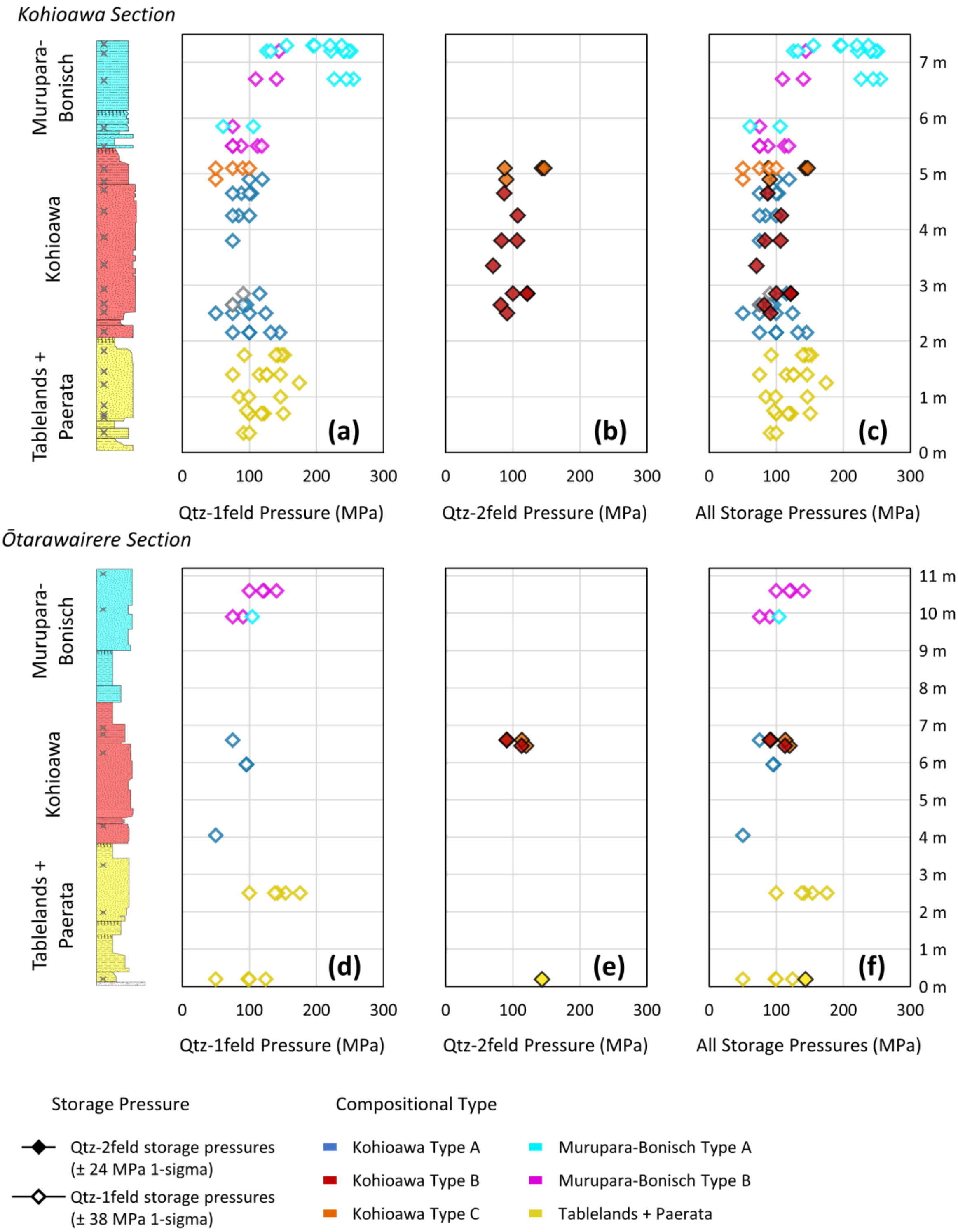

Figure 8 Rhyolite-MELTS storage pressures for glass from pumice clasts of the Kohioawa (top panels) and Ōtarawairere (bottom panels) sections as a function of height through the sections. All pressures are reported in MPa. Left panels (a and d)

show pre-eruptive storage pressures for clasts that returned qtz-1feld (quartz+plagioclase) pressures. Middle panels (b and e) show pre-eruptive storage pressures for clasts that returned qtz-2feld (quartz+plagioclase+sanidine) pressures. Right panels (c and f) show all pressures, with filled diamonds representing qtz-2feld solutions and open diamonds representing qtz-1feld solutions. The Tablelands and Paerata unit yields exclusively qtz-1feld solutions, with resulting pressures similar to those seen in Kohioawa units; note the similarity in pressures between qtz-1feld and qtz-2feld solutions for the Kohioawa unit; for Kohioawa type C, all three pressures ≤ 75 MPa are qtz-1feld pressures; the Murupara-Bonisch unit yields only qtz-1feld solutions, with significantly deeper inferred magma storage conditions for Murupara-Bonisch type A.

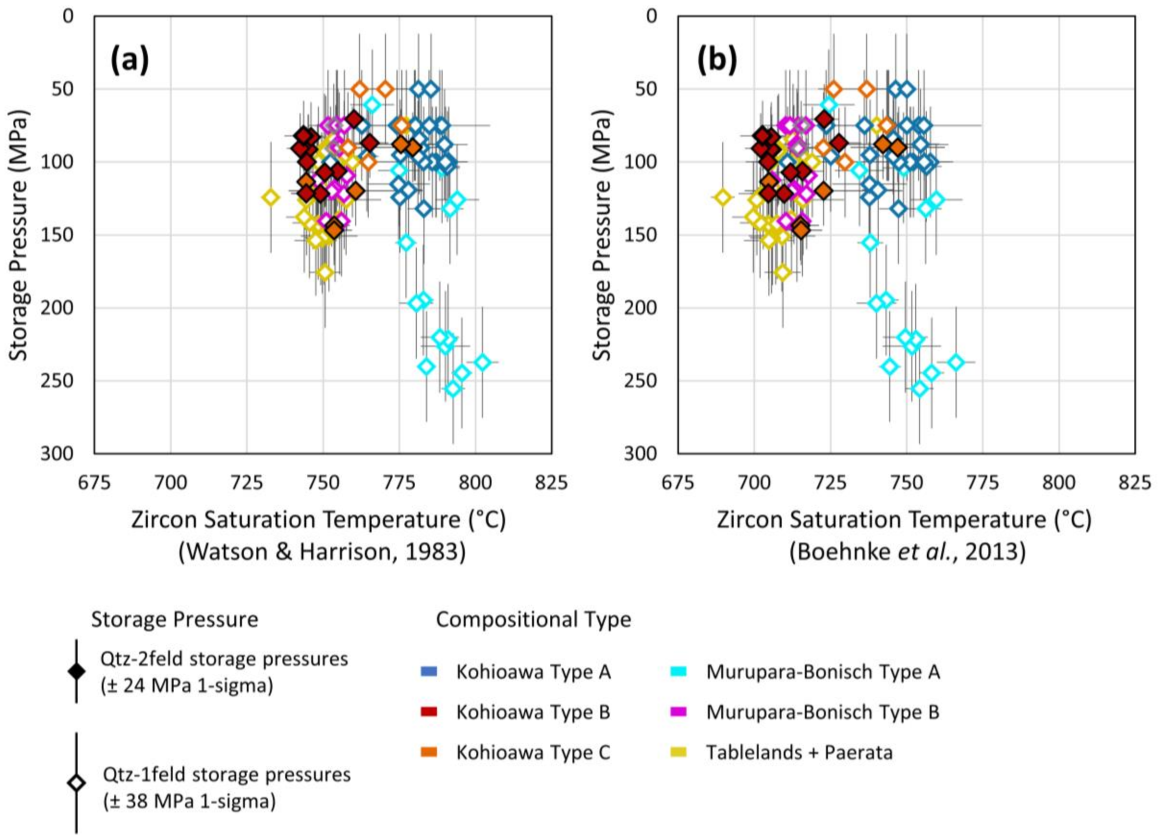

Figure 9 Binary diagrams comparing calculated rhyolite-MELTS storage pressures and zircon-saturation temperatures for average glass compositions from pumice clasts of the Kohioawa and Ōtarawairere sections. Temperatures are calculated using a) the Watson & Harrison (1983) calibration and b) the Boehnke *et al.* (2013) calibration. Note that Kohioawa type A have storage temperatures ~20 °C higher than Kohioawa types B and C, despite similar storage pressures. The symbology is the same as in Figure 8.

DISCUSSION

Magma types and different units

We interpret each clast as a small parcel of magma erupted but not fully fragmented during eruption. Glass compositions allow us to distinguish six compositional types in the clasts, which we interpret to represent six different types of magma that sourced the eruptions.

The glass from each of the three main units (Tablelands and Paerata; Kohioawa; Murupara-Bonisch) has a unique compositional signature (Figures 3-5), consistent with the interpretation of Manning (1995) that these units were sourced from different volcanic centers. Our sampling of multiple horizons allows us to constrain the compositional boundaries, even where paleosols are not present. The lowermost units include a single type of magma that erupted to form the Tablelands B, Tablelands D, and Paerata tephras; the middle unit – which overlies the thickest paleosol – includes three distinct magma types that make up the Kohioawa tephras; and, finally, the topmost unit includes two distinct magma types that make up the Murupara-Bonisch tephras.

In the Kohioawa and Murupara-Bonisch units, multiple magma types are often found within the same horizon. The three different chemical compositions recognized in the Kohioawa unit and two additional types recognized in the Murupara-Bonisch unit indicate that multiple melt-dominated magma bodies erupted simultaneously, similar to some other large eruptions; e.g., the Mamaku and Ohakuri paired eruption (Bégué *et al.*, 2014a, Smithies *et al.*, 2023) and Kidnappers eruption (Cooper *et al.*, 2012), TVZ, New Zealand; Snake River Plain, USA (Ellis and Wolff, 2012; Swallow *et al.*, 2018); Bishop Tuff, Long Valley Caldera, USA (Gualda and Ghiorso, 2013; Gualda *et al.,* 2022); Tokachi and Tokachi-Mitsumata eruptions in central Hokkaido, Japan (Pitcher *et al.*, 2021). The lack of widespread evidence for mixing or mingling on the clast-scale suggests that the contemporaneous melt-dominated magma bodies were stored independently from one another and did not interact prior to or during eruption.

The paleosols within the sequences indicate significant time breaks between eruptions (Manning, 1995). It is difficult to constrain the duration of paleosol development but their thicknesses (e.g., ~40 cm at the top of the Paerata unit at the Ōtarawairere section and ~15 cm at the top of the Kohioawa unit at the Kohioawa section) suggest hiatuses of hundreds to thousands of years (Shoji *et al.*, 1994). After each paleosol, there is a change in glass composition that represents the onset of new magma types.

The transitions in grain size within units (e.g., 480-550 cm in the more massive Kohioawa section, the uppermost Kohioawa package defined by thinner horizons; Figures 1 and 2 and Supplementary tables) indicate changes in eruption intensity for several of the eruptions (Houghton and Carey, 2015). There are two horizons at the Kohioawa section (one from 50-180 cm within the Paerata unit, the other 240-480 cm in the Kohioawa unit; Figure 2) that are much thicker and have relatively larger clasts (fine lapilli) than the other horizons, indicating more sustained, potentially Plinian-style eruptions. Within the Kohioawa unit, at two of these transitions in grain size, there are also discernable differences in magma composition – the addition of Kohioawa type B magma (240 cm) and of Kohioawa Type C magma (480 cm) – suggesting that the change in eruption dynamics could be related to a substantive change in the nature of the magmas erupted.

Correlating the Kohioawa tephra with the Whakamaru group ignimbrites

Previous studies have proposed a correlation between the Kohioawa tephra and the Whakamaru group ignimbrites (Manning, 1995, 1996), and likewise other studies have linked the Rangitawa tephra to the Whakamaru group ignimbrites (Froggatt *et al.*, 1986; Kohn *et al.*, 1992; Pillans *et al.*, 1996; Matthews *et al.*, 2012b). Here, we provide further evidence from published TVZ glass compositions (Bégué *et al.*, 2014b; Gualda *et al.*, 2018) to confirm and strengthen this correlation (Figures 3-5, 10). We demonstrate that the Kohioawa tephras are correlative with the Whakamaru group ignimbrites and are distinct from other TVZ magmas (Deering *et al.*, 2010).

The Rangitawa tephra is described as a pyroclastic fall deposit that has a minimum volume estimate of ~400 km^3 DRE (Matthews *et al.*, 2012b) and has been previously correlated with the widespread Whakamaru group ignimbrites (Kohn *et al.*, 1992; Alloway *et al.*, 1993; Pillans *et al.*, 1996; Lowe *et al.*, 2001; Matthews *et al.*, 2012b, 2012a). Matthews *et al.* (2012b) emphasize that the distal Rangitawa tephra, which is interpreted to represent the Plinian eruption phase, is compositionally similar to Whakamaru type A pumice from Brown *et al*. (1998), which is found in both the Whakamaru and Rangitaiki ignimbrites (Brown *et al.*, 1998; Matthews *et al.*, 2012b). Rangitawa tephra data overlap with our Kohioawa type A glass in both major- and trace-element compositions (Figures 3-5, 10).

By comparing our tephra data with published TVZ major- and trace-element glass data (Figure 10), we find that Kohioawa tephra glass compositions can be distinguished from other TVZ compositions. While Kohioawa type A is more similar to the other TVZ data, it does overlap with the Rangitawa tephra compositions (Matthews *et al.*, 2012b). In particular, Kohioawa types B and C overlap with the Whakamaru ignimbrite data (Bégué *et al.*, 2014b; Gualda *et al.*, 2018), which are compositionally distinct from all other TVZ magmas, likely due to saturation in sanidine (Brown *et al.*, 1998; Gualda *et al.*, 2018).

In addition to the chemical comparisons, the field relations provide further evidence of the correlations. The Matahina ignimbrite overlies the Murupara-Bonisch tephra in the Kohioawa section, so the Kohioawa tephra must be older than the Matahina ignimbrite (i.e., >322 ka). Within the Kohioawa unit, the lack of a paleosol indicates that the tephras were deposited without significant (100s to 1000s a) time breaks, which is consistent with the overlapping Ar-Ar ages of the Whakamaru group ignimbrites (with the exception of the Paeroa Subgroup, as discussed above; see Downs et al., 2014). We thus concur with Manning (1995, 1996) that the Kohioawa tephra has the correct age and composition to be correlative with the ~349 ka Whakamaru group ignimbrites.

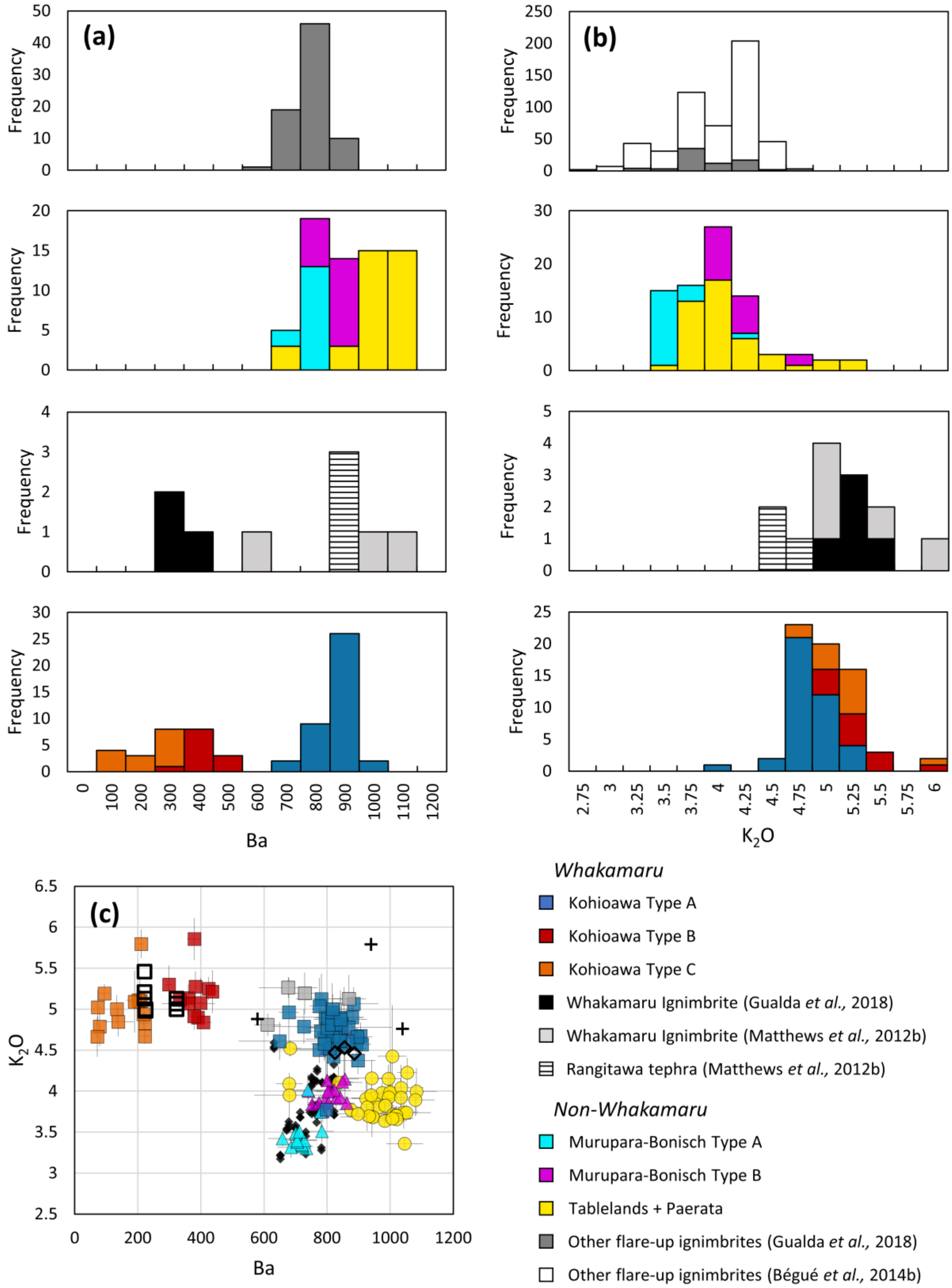

(a)
(b)
(c)
Frequency
Ba
K2O
Whakamaru
Kohioawa Type A
Kohioawa Type B
Kohioawa Type C
Whakamaru Ignimbrite (Gualda et al., 2018)
Whakamaru Ignimbrite (Matthews et al., 2012b)
Rangitawa tephra (Matthews et al., 2012b)
Non-Whakamaru
Murupara-Bonisch Type A
Murupara-Bonisch Type B
Tablelands + Paerata
Other flare-up ignimbrites (Gualda et al., 2018)
Other flare-up ignimbrites (Bégué et al., 2014b)

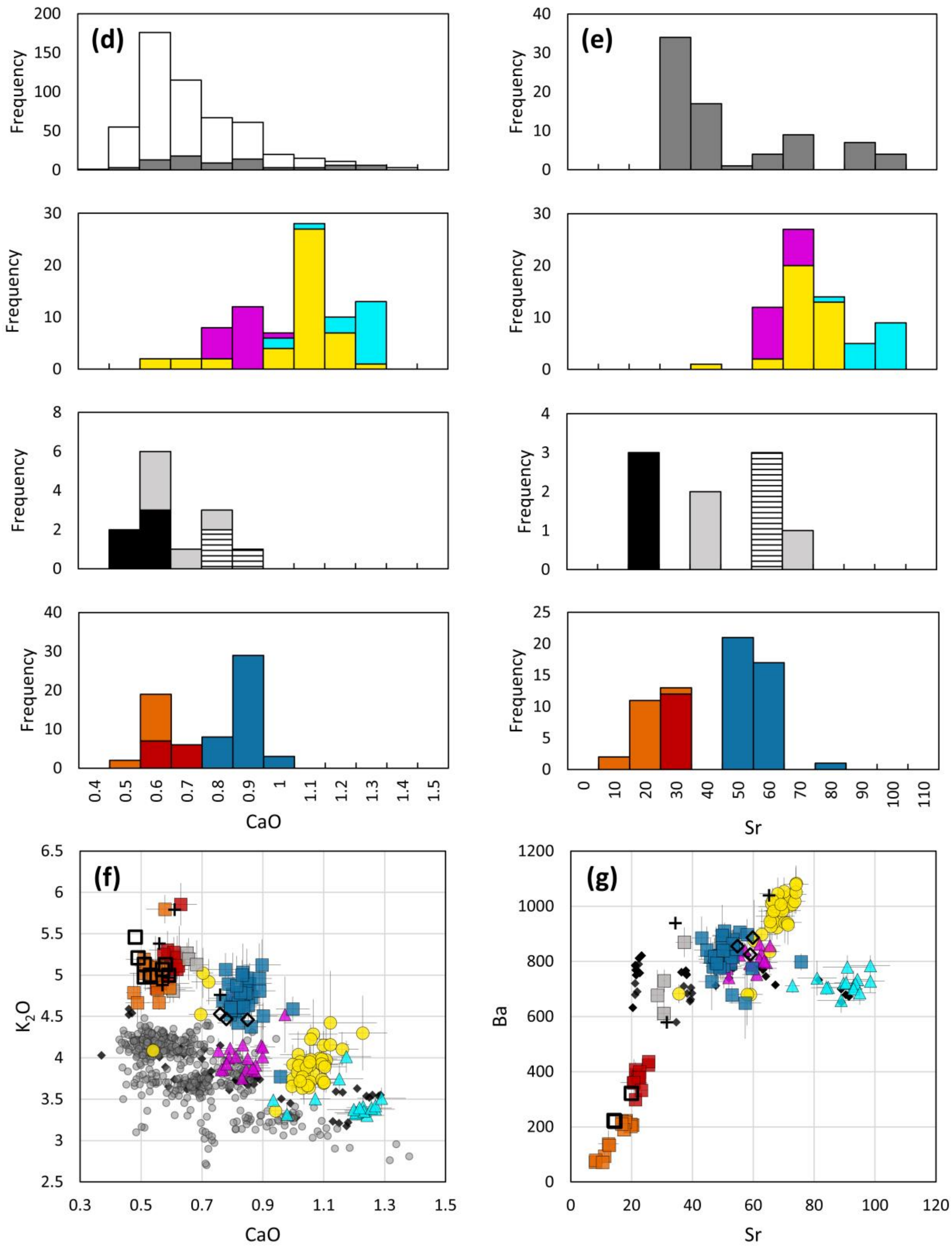

Figure 10 Histograms (a, b, d, e) and binary diagrams (c, f, g) comparing data from the Kohioawa unit (this work), Whakamaru ignimbrites (literature), other tephra units

from the studied tephras (this work), and other units from the TVZ (literature). Data from this work are shown in colors, while data from the literature are shown in grayscale. The symbology in the binary diagrams is the same as in Figures 3-5. Ba and K_2O distributions show that Whakamaru and Kohioawa compositions are distinct from other TVZ compositions and demonstrate that the Kohioawa unit corresponds to tephras correlative with the Whakamaru group ignimbrites.

Kohioawa magmas and the Whakamaru group eruptions

Brown *et al*. (1998) describe four magma types in the Whakamaru group eruptions, based on whole-rock and glass analyses from single pumice clasts. Types A, B, and C observed by us in the Kohioawa tephras match types A, B, and C from Brown *et al*. (1998). We cannot effectively distinguish type D from type A using glass data alone.

The Kohioawa tephras provide a more complete record of the fall deposits formed by the Whakamaru eruptions than the Rangitawa tephras do, as the Rangitawa tephras only include type A magmas. The single horizon in the Kohioawa tephra that includes only type A magma is the basal subunit; we, thus, suggest that the widespread Rangitawa tephra is equivalent to the basal package of the Kohioawa tephra, which represents the initial eruption stage of the Whakamaru group. While this is corroborated by the geochemical observations of Matthews *et al.* (2012b), it contrasts with their interpretation that the Rangitawa tephra correlates with a later stage of the Whakamaru eruptions (Matthews *et al.*, 2012b).We note that no fall deposit has been found under or within the Whakamaru ignimbrite (*sensu stricto)*, so characterizing the tephra deposits as “Plinian” or “co-ignimbrite” is not yet definitive.

Multiple eruptive pulses could reconcile previous work, which are contrasting in the interpretations of one versus multiple eruptions. Some previous studies describe the different ignimbrites as potentially different eruptions (Grindley, 1960; Martin, 1961; Briggs, 1976a, 1976b; Wilson *et al.*, 1986), while more recent work describes a single complex eruption episode for the Whakamaru group ignimbrites (with the Paeroa Subgroup as a second, ~10 ka younger eruption) (Brown *et al.*, 1998; Downs *et al.*, 2014). The lack of a paleosol within the Kohioawa tephras indicates that any break within the Whakamaru group eruptions would have to have been short, and likely not discernible via Ar-Ar ages (Downs *et al.*, 2014). However, the three distinct packages of the Kohioawa unit reveal three major eruptive phases of the Whakamaru group eruptions.

Kohioawa type A is the exclusive magma type present in the lowest Kohioawa package, which is consistent with the interpretation that sanidine was absent in the early stages of the Whakamaru group ignimbrites (Ewart, 1965; Brown *et al.*, 1998). Kohioawa types A and B are present in approximately equal proportions in the middle package; and all three types are present in the uppermost package, where Kohioawa type C dominates, as indicated by the lower Sr and Ba signatures in the glass. The presence of sanidine-bearing Kohioawa type B from the second package through the top of the sequence indicates that only the first phase of the eruptions lacked sanidine, consistent with the mineralogy observations of the various horizons and by rhyolite-MELTS calculations. This shift to include Kohioawa type C indicates that the final phase of the eruptions included more evolved magmas than what is observed over the majority of the eruptions. Each clast has a distinct compositional signature, precluding any chemical mixing on the ash-to-lapilli-scale prior to or during eruption.

Storage conditions and architecture of the Whakamaru magma bodies

The tephra data show that three distinct magma types fed the Whakamaru group eruptions: Kohioawa types A, B, and C. All three Kohioawa magma types are stored at the same shallow pre-eruptive storage pressures (50-150 MPa), indicating that the magma bodies coexisted at the same pre-eruptive storage depth within the crust (Figure 11). The Kohioawa types B and C magmas likely have a tightly constrained storage pressure, as most of the pressures are constrained to ~70-150 MPa and these storage pressures exhibit predominantly qtz-2feld pressures that include quartz+plagioclase+sanidine, which have smaller uncertainties of ± 24 MPa 1-sigma (Pitcher *et al.*, 2021), whereas the Kohioawa type A magma has a wider storage range of 50-150 MPa and exhibit qtz-1feld pressures that do not include sanidine in the assemblage.

Our storage pressures are in contrast with the model of Brown *et al*. (1998), which envisioned a single, stratified magma body, with three main types of magma that are connected (Whakamaru types A, B, and C), forming a zoned magma body with the most fractionated magma at the top of the magma body, with crystal fractionation playing a dominant role in differentiating magma types. Since all Kohioawa types yield overlapping storage pressures and both types A and B erupted continuously throughout most of the eruption, our data are inconsistent with the presence of a single zoned magma body.

Further evidence for the presence of multiple melt-dominated magma bodies is provided by zircon saturation temperatures, as the difference in temperatures implies that the eruptions could not be sourced from a single, zoned magma chamber (Figure 9). As well, the Zr concentrations we document further demonstrate that type A magmas are compositionally distinct from types B and C, reinforcing the idea that they represent different magma bodies.

The continuous deposition of both Kohioawa types A and B in the middle and uppermost Kohioawa packages indicates that both magma types erupted simultaneously and continuously throughout the eruption. They likely erupted from two separate, laterally juxtaposed melt-dominated magma bodies that were tapped during most of the eruptive event. The overlap in storage pressures and temperatures indicates that there is likely a segregated melt-dominated magma body that erupted Kohioawa type C independent from and laterally juxtaposed to Kohioawa type B in the final stages of the eruptions. While Kohioawa type C magma could be genetically related to Kohioawa type B magma (with type C being similar but more fractionated than type B), the processes linking the two magma types deserve further study.

Tephra compositions and calculated storage pressures show that each magma type displays a narrow compositional range and erupts from a narrow pressure range (Figure 11). Most units show storage pressures of 75-150 MPa (~ 3-6 km), indicating a consistent and narrow storage zone within the shallow crust that is repeated through the eruptions. Given that this pressure interval prevails over most of the eruptions studied here, it seems likely that a rheological (e.g., Huber *et al.*, 2019), structural, or tectonic factor (or a combination of factors) controls the storage level of these magmas. This is consistent with what can be inferred from the results of Bégué *et al*. (2014b) for the central TVZ as a whole (see also Cooper *et al.*, 2012; Allan *et al.*, 2013).

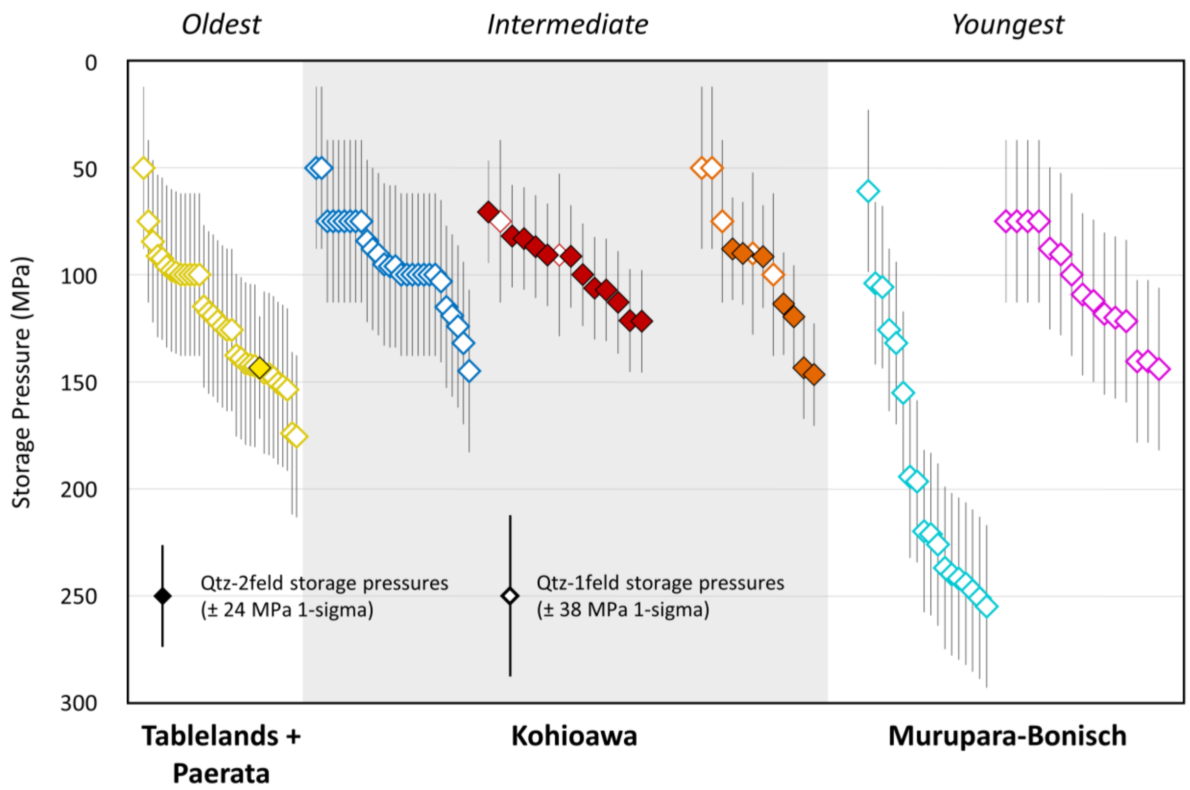

Figure 11 Rank order diagram of rhyolite-MELTS storage pressures. Qtz-1feld pressure results are indicated by open diamond symbols, and qtz-2feld pressure results are indicated by filled diamond symbols; the different compositional types are indicated by the different colors. The one-sigma uncertainties for the qtz-1feld and qtz-2feld pressure calculations are shown. The Tablelands and Paerata unit (oldest in the sequence) appears on the left; the Kohioawa unit appears in the middle portion of the figure; the Murupara-Bonisch unit (youngest in the sequence) appears on the right. There could be multiple magma bodies for a given magma type. There is one magma type that contributed to the Tablelands and Paerata tephras, three magma types that contributed to the Kohioawa tephras (which are correlative with the Whakamaru eruptions), and two magma types that contributed to the Murupara-Bonisch tephras.

The Whakamaru eruptions commenced with the Kohioawa type-A magma and erupted both types A (blue) and B (red) for most of the eruptions, and erupted types A, B, and C (orange) in the final stages of the Whakamaru eruptions.

CONCLUSIONS

In this work, we use a combination of field and analytical techniques to characterize two tephra sequences in the Bay of Plenty, Aotearoa New Zealand, focusing on glass geochemistry and determination of crystallization conditions using rhyolite-MELTS geobarometry and zircon-saturation geothermometry.

We leverage the unique mineralogy and glass compositions of Whakamaru magmas to demonstrate that the Kohioawa unit is correlative with the Whakamaru ignimbrites and the Rangitawa tephra, consistent with previous studies (Froggatt *et al.*, 1986; Kohn *et al.*, 1992; Pillans *et al.*, 1996; Brown *et al.*, 1998; Matthews *et al.*, 2012b). Combining volcanological information from the tephras with petrological inferences using glass compositions, we provide new information on the eruptive history and the architecture of the Whakamaru magmatic system.

During the initial stages of the Whakamaru group eruptions, only type A magmas erupted, suggesting that the Rangitawa tephras are correlative with this phase of the eruptions. Following this initial event, Kohioawa type A and B magmas erupted continuously through most of the Kohioawa sequence, suggesting the presence of at least two independent magma bodies (one sanidine-absent, and one sanidine -bearing) for most of the duration of the eruptions. The final stages of the Kohioawa unit include an additional third magma type (type C). This indicates a shift in the final stages of the eruptions to include a third magma body.

Our data do not support the model of Brown *et al*. (1998) of a single, vertically stratified magma body. Instead, our data suggest the presence of likely three laterally juxtaposed and chemically independent magma bodies. These bodies appear to have been stored primarily at a pressure range of 50-150 MPa (depths of ~2-6 km).

The younger Murupara-Bonisch tephras show a significant change in composition, and the eruption of different magma types sourced from different storage levels. Even though they are sourced from the Ōkataina volcanic center, the dramatic shift in composition between Whakamaru-related magmas and Murupara-Bonisch magmas shows that the central TVZ magma systems went through a thorough reorganization following the Whakamaru event (Gravley *et al.*, 2016; Gualda *et al.*, 2018).

Data from tephra units allow us to identify the number of melt-dominated magma bodies that existed prior to the Whakamaru eruption(s), as well as the smaller eruptions that preceded and postdated this massive event. The inferred storage conditions (pressures and temperatures) indicate a network of co-erupting melt-dominated magma bodies that fed the eruption(s), as has been documented for some other large eruptions (e.g., Gravley *et al.*, 2007; Cooper *et al.*, 2012; Gualda and Ghiorso, 2013; Bégué *et al.*, 2014a; Cashman and Giordano, 2014; Cooper, 2017; Swallow *et al.*, 2018; Gualda *et al.*, 2022). The relative ages of the tephra units allow us to identify when different magma types started and stopped erupting through time. Identifying the number and depths of melt-dominated magma bodies provides insight about their possible arrangement in the shallow crust prior to large eruptions, and how they can impact the storage conditions of magma evacuated in subsequent eruptions. The complementary record of the tephras adds to our understanding of the ignimbrite eruptions, especially in cases where the field relations are complex.

ACKNOWLEDGEMENTS

We would like to thank Ayla Pamukçu and Elizabeth Grant for help during field work in 2017. Thank you to Mark Ghiorso, Calvin Miller, Ayla Pamukçu, Bradley Pitcher, and Christy Till for advice on earlier drafts of the manuscript. Constructive reviews kindly provided by Steve Self and Lorenzo Tavazzani. This work was supported by the National Science Foundation [EAPSI-1714025 to L.J.H, EAR-1830122 to G.A.R.G.].

DATA AVAILABILITY STATEMENT

The quantitative data underlying this article and detailed methods are available in the article and in its online supplementary material. SEM BSE images of clasts will be shared on reasonable request to the corresponding author.

REFERENCES

Allan, A. S. R., Barker, S. J., Millet, M. A., Morgan, D. J., Rooyakkers, S. M., Schipper, C. I. & Wilson, C. J. N. (2017). A cascade of magmatic events during the assembly and eruption of a super-sized magma body. *Contributions to Mineralogy and Petrology* **172**, 49.

Allan, A. S. R., Morgan, D. J., Wilson, C. J. N. & Millet, M. A. (2013). From mush to eruption in centuries: Assembly of the super-sized Oruanui magma body. *Contributions to Mineralogy and Petrology* **166**, 143–164.

Alloway, B. V., Pillans, B. J., Sandhu, A. S. & Westgate, J. A. (1993). Revision of the marine chronology in the Wanganui Basin, New Zealand, based on the isothermal plateau fission-track dating of tephra horizons. *Sedimentary Geology* **82**, 299–310.

Bachmann, O. & Bergantz, G. W. (2004). On the origin of crystal-poor rhyolites: Extracted from batholithic crystal mushes. *Journal of Petrology* **45**, 1565–1582.

Bachmann, O. & Bergantz, G. W. (2008). The magma reservoirs that feed supereruptions. *Elements* **4**, 17–21.

Bailey, R. A. & Carr, R. G. (1994). Physical geology and eruptive history of the Matahina Ignimbrite, Taupo Volcanic Zone, North Island, New Zealand. *New Zealand Journal of Geology and Geophysics* **37**, 319–344.

Barboni, M., Annen, C. & Schoene, B. (2015). Evaluating the construction and evolution of upper crustal magma reservoirs with coupled U/Pb zircon geochronology and thermal modeling: A case study from the Mt. Capanne pluton (Elba, Italy). *Earth and Planetary Science Letters* **432**, 436–448.

Bégué, F., Deering, C. D., Gravley, D. M., Kennedy, B. M., Chambefort, I., Gualda, G. A. R. & Bachmann, O. (2014a). Extraction, storage and eruption of multiple isolated magma batches in the paired Mamaku and Ohakuri eruption, Taupo Volcanic Zone, New Zealand. *Journal of Petrology* **55**, 1653–1684.

Bégué, F., Gualda, G. A. R., Ghiorso, M. S., Pamukçu, A. S., Kennedy, B. M., Gravley, D. M., Deering, C. D. & Chambefort, I. (2014b). Phase-equilibrium geobarometers for silicic rocks based on rhyolite-MELTS. Part 2: application to Taupo Volcanic Zone rhyolites. *Contributions to Mineralogy and Petrology* **168**, 1–16.

Blundy, J. D. & Cashman, K. V. (2008). Petrologic reconstruction of magmatic system variables and processes. *Reviews in Mineralogy & Geochemistry* **69**, 179–239.

Boehnke, P., Watson, E. B., Trail, D., Harrison, T. M. & Schmitt, A. K. (2013). Zircon saturation re-revisited. *Chemical Geology* **351**, 324–334.

Bonadonna, C., Costa, A., Folch, A. & Koyaguchi, T. (2015). Chapter 33 - Tephra Dispersal and Sedimentation. In: Sigurdsson, H., *et al.* (eds.) *The Encyclopedia of Volcanoes (Second Edition).* Academic Press, 587–597.

Bonadonna, C. & Phillips, J. C. (2003). Sedimentation from strong volcanic plumes. *Journal of Geophysical Research: Solid Earth* **108**, B7, 2340.

Briggs, N. D. (1976a). Recognition and correlation of subdivisions within the Whakamaru ignimbrite, central North Island, New Zealand. *New Zealand Journal of Geology and Geophysics* **19**, 463–501.

Briggs, N. D. (1976b). Welding and crystallisation zonation in Whakamaru Ignimbrite, central North Island, New Zealand. *New Zealand Journal of Geology and Geophysics* **19**, 189–212.

Brown, R. J., Bonadonna, C. & Durant, A. J. (2012). A review of volcanic ash aggregation. *Physics and Chemistry of the Earth* **45–46**, 65–78.

Brown, S. J. A. & Fletcher, I. R. (1999). SHRIMP U-Pb dating of the preeruption growth history of zircons from the 340 ka Whakamaru Ignimbrite, New Zealand: Evidence for >250 k.y. magma residence times. *Geology* **27**, 1035–1038.

Brown, S. J. A., Wilson, C. J. N., Cole, J. W. & Wooden, J. L. (1998). The Whakamaru group ignimbrites, Taupo Volcanic Zone, New Zealand: Evidence for reverse tapping of a zoned silicic magmatic system. *Journal of Volcanology and Geothermal Research* **84**, 1–37.

Cashman, K. V. & Giordano, G. (2014). Calderas and magma reservoirs. *Journal of Volcanology and Geothermal Research* **288**, 28–45.

Chambefort, I., Lewis, B., Wilson, C. J. N., Rae, A. J., Coutts, C., Bignall, G. & Ireland, T. R. (2014). Stratigraphy and structure of the Ngatamariki geothermal system from new zircon U–Pb geochronology: Implications for Taupo Volcanic Zone evolution. *Journal of Volcanology and Geothermal Research* **274**, 51–70.

Chamberlain, K. J., Wilson, C. J. N., Wallace, P. J. & Millet, M. A. (2015). Micro-analytical perspectives on the Bishop Tuff and its magma chamber. *Journal of Petrology* **56**, 605–640.

Charlier, B. L. A., Bachmann, O., Davidson, J. P., Dungan, M. A. & Morgan, D. J. (2007). The upper crustal evolution of a large silicic magma body: Evidence from crystal-scale Rb-Sr isotopic heterogeneities in the Fish Canyon magmatic system, Colorado. *Journal of Petrology* **48**, 1875-1894.

Cooper, G. F., Morgan, D. J. & Wilson, C. J. N. (2017). Rapid assembly and rejuvenation of a large silicic magmatic system: Insights from mineral diffusive profiles in the Kidnappers and Rocky Hill deposits, New Zealand. *Earth and Planetary Science Letters* **473**, 1–13.

Cooper, G. F., Wilson, C. J. N., Millet, M. A., Baker, J. A. & Smith, E. G. C. (2012). Systematic tapping of independent magma chambers during the 1Ma Kidnappers supereruption. *Earth and Planetary Science Letters* **313–314**, 23–33.

Cooper, K. M. (2017). What does a magma reservoir look like? The "crystal's-eye" view. *Elements* **13**, 23–28.

Cooper, K. M. & Kent, A. J. R. (2014). Rapid remobilization of magmatic crystals kept in cold storage. *Nature* **506**, 480–483.

Costa, A., Folch, A., Macedonio, G., Giaccio, B., Isaia, R. & Smith, V. C. (2012). Quantifying volcanic ash dispersal and impact of the Campanian Ignimbrite super-eruption. *Geophysical Research Letters* **39**, L10310.

Deering, C. D., Bachmann, O. & Vogel, T. A. (2011). The Ammonia Tanks Tuff: Erupting a melt-rich rhyolite cap and its remobilized crystal cumulate. *Earth and Planetary Science Letters* **310**, 518–525.

Deering, C. D., Gravley, D. M., Vogel, T. A., Cole, J. W. & Leonard, G. S. (2010). Origins of cold-wet-oxidizing to hot-dry-reducing rhyolite magma cycles and distribution in the Taupo Volcanic Zone, New Zealand. *Contributions to Mineralogy and Petrology* **160**, 609–629.

Downs, D. T., Wilson, C. J. N., Cole, J. W., Rowland, J. V., Calvert, A. T., Leonard, G. S. & Keall, J. M. (2014). Age and eruptive center of the Paeroa Subgroup ignimbrites

(Whakamaru Group) within the Taupo Volcanic Zone of New Zealand. *Bulletin of the Geological Society of America* **126**, 1131–1144.

Druitt T. H., Costa F., Deloule E., Dungan M., Scaillet B. (2012) Decadal to monthly timescales of magma transfer and reservoir growth at a caldera volcano. *Nature* 482, 77–80.

Eastwood, A. A., Gravley, D. M., Wilson, C. J. N., Chambefort, I., Oze, C., Cole, J. W. & Ireland, T. R. (2013). U-Pb dating of subsurface pyroclastic deposits (Tahorakuri Formation) at Ngatamariki and Rotokawa Geothermal Fields. Proceedings, *35th New Zealand Geothermal Workshop*. Rotorua, New Zealand.

Ellis, B. S. & Wolff, J. A. (2012). Complex storage of rhyolite in the central Snake River Plain. *Journal of Volcanology and Geothermal Research* **211–212**, 1–11.

Ewart, A. (1965). Mineralogy and petrogenesis of the Whakamaru ignimbrite in the Maraetai area of the Taupo volcanic zone, New Zealand. *New Zealand Journal of Geology and Geophysics* **8**, 611–679.

Ewart, A. & Healy, J. (1966). Te Whaiti ignimbrites at Murupara. In: Thompson, B., Kermode, L. & Ewart, A. (eds) *New Zealand Volcanology, Central Volcanic Region*. New Zealand Department of Scientific and Industrial Research Information, 121–125.

Folch, A. & Felpeto, A. (2005). A coupled model for dispersal of tephra during sustained explosive eruptions. *Journal of Volcanology and Geothermal Research* **145**, 337–349.

Foley, M. L., Miller, C. F. & Gualda, G. A. R. (2020). Architecture of a super-sized magma chamber and remobilization of its basal cumulate (Peach Spring Tuff, USA). *Journal of Petrology* **61**, egaa020.

Froggatt, P., Nelson, C., Carter, L., Griggs, G. & Black, K. (1986). An exceptionally large late Quaternary eruption from New Zealand. *Nature* **319**, 578–582.

Gravley, D. M., Deering, C. D., Leonard, G. S. & Rowland, J. V. (2016). Ignimbrite flare-ups and their drivers: A New Zealand perspective. *Earth-Science Reviews* **162**, 65–82.

Gravley, D. M., Wilson, C. J. N., Leonard, G. S. & Cole, J. W. (2007). Double trouble: Paired ignimbrite eruptions and collateral subsidence in the Taupo Volcanic Zone, New Zealand. *Bulletin of the Geological Society of America* **119**, 18–30.

Grindley, G. (1960). Geological Map of New Zealand 1:250,000. *NZ Department of Scientific and Industrial Research*. Wellington, New Zealand.

Gualda, G. A. R. & Ghiorso, M. S. (2013). The Bishop Tuff giant magma body: an alternative to the Standard Model. *Contributions to Mineralogy and Petrology* **166**, 755–775.

Gualda, G. A. R. & Ghiorso, M. S. (2014). Phase-equilibrium geobarometers for silicic rocks based on rhyolite-MELTS. Part 1: Principles, procedures, and evaluation of the method. *Contributions to Mineralogy and Petrology* **168**, 1–17.

Gualda, G. A. R. & Ghiorso, M. S. (2015). MELTS-Excel: A Microsoft Excel-based MELTS interface for research and teaching of magma properties and evolution. *Geochemistry, Geophysics, Geosystems* **16**, 315–324.

Gualda, G. A. R., Ghiorso, M. S., Hurst, A. A., Allen, M. C. & Bradshaw, R. W. (2022). A complex patchwork of magma bodies that fed the Bishop Tuff supereruption (Long Valley Caldera, CA, United States): Evidence from matrix glass major and trace-element compositions. *Frontiers in Earth Science* **10**.

Gualda, G. A. R., Ghiorso, M. S., Lemons, R. V. & Carley, T. L. (2012a). Rhyolite-MELTS: a modified calibration of MELTS optimized for silica-rich, fluid-bearing magmatic systems. *Journal of Petrology* **53**, 875–890.

Gualda, G. A. R., Gravley, D. M., Conner, M., Hollmann, B., Pamukçu, A. S., Bégué, F., Ghiorso, M. S. & Deering, C. D. (2018). Climbing the crustal ladder: Magma storage-depth evolution during a volcanic flare-up. *Science Advances* **4**, eaap7567.

Gualda, G. A. R., Pamukçu, A. S., Ghiorso, M. S., Anderson Jr, A. T., Sutton, S. R. & Rivers, M. L. (2012b). Timescales of quartz crystallization and the longevity of the Bishop giant magma body. *PLoS ONE* **7**, e37492.

Gualda, G. A. R. & Sutton, S. R. (2016). The year leading to a supereruption. *PLoS ONE* **11**, 1–18.

Harmon, L. J., Cowlyn, J., Gualda, G. A. R. & Ghiorso, M. S. (2018). Phase-equilibrium geobarometers for silicic rocks based on rhyolite-MELTS. Part 4: Plagioclase, orthopyroxene, clinopyroxene, glass geobarometer, and application to Mt. Ruapehu, New Zealand. *Contributions to Mineralogy and Petrology* **173**, 7.

Healy, J., Schofield, J. & Thompson, B. (1964). *Sheet 5, Rotorua. Geological Map of New Zealand 1:250,000*. Wellington.

Hildreth, W. (1979). The Bishop Tuff: Evidence for the origin of compositional zonation in silicic magma chambers. *Geological Society of America* **180**, 43-75.

Hildreth, W. & Wilson, C. J. N. (2007). Compositional zoning of the Bishop Tuff. *Journal of Petrology* **48**, 951–999.

Holt, K. A., Wallace, R. C., Neall, V. E., Kohn, B. P. & Lowe, D. J. (2010). Quaternary tephra marker beds and their potential for palaeoenvironmental reconstruction on Chatham Island, east of New Zealand, southwest Pacific Ocean. *Journal of Quaternary Science* **25**, 1169–1178.

Houghton, B. & Carey, R. J. (2015). Chapter 34 - Pyroclastic Fall Deposits. In: Sigurdsson, H. (ed.) *The Encyclopedia of Volcanoes (Second Edition)*. Amsterdam: Elsevier, 599–616.

Houghton, B. F., Wilson, C. J. N., McWilliams, M. O., Lanphere, M. A., Weaver, S. D., Briggs, R. M. & Pringle, M. S. (1995). Chronology and dynamics of a large silicic magmatic system: Central Taupo Volcanic Zone, New Zealand. *Geology* **23**, 13–16.

Huber, C., Townsend, M., Degruyter, W., Bachmann O. (2019) Optimal depth of subvolcanic magma chamber growth controlled by volatiles and crust rheology. *Nature Geoscience* **12**, 762–768.

Kaiser, J. F., de Silva, S., Schmitt, A. K., Economos, R. & Sunagua, M. (2017). Million-year melt–presence in monotonous intermediate magma for a volcanic–plutonic assemblage in the Central Andes: Contrasting histories of crystal-rich and crystal-poor super-sized silicic magmas. *Earth and Planetary Science Letters* **457**, 73–86.

Kohn, B. P., Pillans, B. & Mcglone, M. S. (1992). Zircon fission track age for middle Pleistocene Rangitawa Tephra, New Zealand: stratigraphic and paleoclimatic significance. *Palaeogeography, Palaeoclimatology, Palaeoecology* **95**, 73–94.

Leonard, G. S., Begg, J. G. & Wilson, C. J. N. (2010). Geology of the Rotorua area. Lower Hutt, New Zealand: GNS Science.

Lipman, P. W. (1965) Chemical comparison of glassy and crystalline volcanic rocks. *Contributions to General Geology, Geological Survey Bulletin* **1201D,** 1-24.

Lowe, D. J., Tippett, J. M., Kamp, P. J. J., Liddell, I. J., Briggs, R. M. & Horrocks, J. L. (2001). Ages on weathered Plio-Pleistocene tephra sequences, western North Island, New Zealand. In: Juvigné, E. T. & Raynal, J-P. (eds) "Tephras: Chronology, Archaeology", CDERAD éditeur, Goudet. *Les Dossiers de l'Archéo-Logis* **1**, 45-60.

Manning, D. A. (1995). Late Pleistocene tephrostratigraphy of the eastern Bay of Plenty region, New Zealand. Wellington, Victoria University.

Manning, D. A. (1996). Middle-late Pleistocene tephrastratigraphy of the eastern Bay of Plenty, New Zealand. *Quaternary International* **34–36**, 3–12.

Martin, R. C. (1961). Stratigraphy and structural outline of the Taupo Volcanic Zone. *New Zealand Journal of Geology and Geophysics* **4**, 449–478.

Martin, R. C. (1965). Lithology and eruptive history of the Whakamaru ignimbrites in the Maraetai area of the Taupo volcanic zone, New Zealand. *New Zealand Journal of Geology and Geophysics* **8**, 680–705.

Matthews, N. E. (2011). Magma chamber assembly and dynamics of a supervolcano: Whakamaru, Taupo Volcanic Zone, New Zealand. Oxford, University of Oxford.

Matthews, N. E., Pyle, D. M., Smith, V. C., Wilson, C. J. N., Huber, C. & van Hinsberg, V. (2012a). Quartz zoning and the pre-eruptive evolution of the ~340-ka Whakamaru magma systems, New Zealand. *Contributions to Mineralogy and Petrology* **163**, 87–107.

Matthews, N. E., Smith, V. C., Costa, A., Durant, A. J., Pyle, D. M. & Pearce, N. J. G. (2012b). Ultra-distal tephra deposits from super-eruptions: Examples from Toba, Indonesia and Taupo Volcanic Zone, New Zealand. *Quaternary International* **258**, 54–79.

Pamukçu, A. S., Carley, T. L., Gualda, G. A. R., Miller, C. F. & Ferguson, C. A. (2013). The evolution of the Peach Spring giant magma body: Evidence from accessory mineral textures and compositions, bulk pumice and glass geochemistry, and rhyolite-MELTS modeling. *Journal of Petrology* **54**, 1109–1148.

Pamukçu, A. S., Gualda, G. A. R., Bégué, F. & Gravley, D. M. (2015a). Melt inclusion shapes: Timekeepers of short-lived giant magma bodies. *Geology* **43**, 947–950.

Pamukçu, A. S., Gualda, G. A. R., Ghiorso, M. S., Miller, C. F. & McCracken, R. G. (2015b). Phase-equilibrium geobarometers for silicic rocks based on rhyolite-MELTS—Part 3: Application to the Peach Spring Tuff (Arizona–California–Nevada, USA). *Contributions to Mineralogy and Petrology* **169**, 1-17.

Pamukçu, A. S., Wright, K. A., Gualda, G. A., & Gravley, D. (2020). Magma residence and eruption at the Taupo Volcanic Center (Taupo Volcanic Zone, New Zealand): insights from rhyolite-MELTS geobarometry, diffusion chronometry, and crystal textures. *Contributions to Mineralogy and Petrology* **175**, 1-27.

Pamukçu, A. S., Gualda, G. A. R. & Gravley, D. M. (2021). Rhyolite-MELTS and the storage and extraction of large-volume crystal-poor rhyolitic melts at the Taupō Volcanic Center: a reply to Wilson et al. (2021). *Contributions to Mineralogy and Petrology* **176**, 1-16.

Pillans, B., Kohn, B. P., Berger, G., Froggatt, P., Duller, G., Alloway, B. & Hesset, P. (1996). Multi-method dating comparison for mid-Pleistocene Rangitawa Tephra, New Zealand. *Quaternary Science Reviews* **15**, 641–653.

Pitcher, B. W., Gualda, G. A. R. & Hasegawa, T. (2021). Repetitive Duality of Rhyolite Compositions, Timescales, and Storage and Extraction Conditions for Pleistocene Caldera-forming Eruptions, Hokkaido, Japan. *Journal of Petrology* **62**, egaa106.

Reid, M. R. & Vazquez, J. A. (2017). Fitful and protracted magma assembly leading to a giant eruption, Youngest Toba Tuff, Indonesia. *Geochemistry Geophysics Geosystems* **18**, 156–177.

Saunders, K., Morgan, D. J., Baker, J. A. & Wysoczanski, R. J. (2010). The Magmatic Evolution of the Whakamaru Supereruption, New Zealand, Constrained by a Microanalytical Study of Plagioclase and Quartz. *Journal of Petrology* **51**, 2465–2488.

Scott, R. (1971) Alkali exchange during devitrification and hydration of glasses in ignimbrite cooling units. *Journal of Geology* **79**, 100-110.

Shamloo, H. I. & Till, C. B. (2019). Decadal transition from quiescence to supereruption: petrologic investigation of the Lava Creek Tuff, Yellowstone Caldera, WY. *Contributions to Mineralogy and Petrology* **174**, 1-18.

Shoji, S., Nanzyo, M. & Dahlgren, R. (1994). *Volcanic Ash Soils: Genesis, Properties and Utilization*. Elsevier: Amsterdam, Netherlands.

Simon, J. I. & Reid, M. R. (2005). The pace of rhyolite differentiation and storage in an “archetypical” silicic magma system, Long Valley, California. *Earth and Planetary Science Letters* **235**, 123–140.

Smithies, S. L., Harmon, L. J., Allen, S. M., Gravley, D. M. & Gualda, G. A. R. (2023). Following magma: The pathway of silicic magmas from extraction to storage during an ignimbrite flare-up, Taupō Volcanic Zone, New Zealand. *Earth and Planetary Science Letters* **607**, 118053.

Stelten, M. E., Cooper, K. M., Vazquez, J. A., Calvert, A. T. & Glessner, J. J. G. (2014). Mechanisms and timescales of generating eruptible rhyolitic magmas at Yellowstone Caldera from Zircon and sanidine geochronology and geochemistry. *Journal of Petrology* **56**, 1607–1642.

Swallow, E. J., Wilson, C. J. N., Myers, M. L., Wallace, P. J., Collins, K. S. & Smith, E. G. C. (2018). Evacuation of multiple magma bodies and the onset of caldera collapse in a supereruption, captured in glass and mineral compositions. *Contributions to Mineralogy and Petrology* **173**, 1–22.

Watson, E. B. & Harrison, T. M. (1983). Zircon saturation revisited: temperature and composition effects in a variety of crustal magma types. *Earth and Planetary Science Letters* **64**, 295–304.

Wilson, C. J. N. & Charlier, B. L. A. (2009). Rapid rates of magma generation at contemporaneous magma systems, Taupo volcano, New Zealand: Insights from U-Th model-age spectra in Zircons. *Journal of Petrology* **50**, 875–907.

Wilson, C. J. N. & Charlier, B. L. A. (2016). The life and times of silicic volcanic systems. *Elements* **12**, 103–108.

Wilson, C. J. N., Gravley, D. M., Leonard, G. S. & Rowland, J. V. (2009). Volcanism in the central Taupo Volcanic Zone, New Zealand: tempo styles and controls. In: Thordarson, T., Self, S., Larsen, G., Rowland, S. K. & Hoskuldsson, A. (eds) *Studies in Volcanology: The Legacy of George Walker*. *Special Publications of IAVCEI*, 225–247.

Wilson, C. J. N., Houghton, B. F. & Lloyd, E. F. (1986). Volcanic history and evolution of the Maroa-Taupo area. In: Smith, I. E. M. (ed.) *Late Cenozioc Volcanism in New Zealand*. Wellington: The Royal Society of New Zealand Bulletin **23**, 194–223.

Wilson, C. J. N., Houghton, B. F., McWilliams, M. O., Lanphere, M. A., Weaver, S. D. & Briggs, R. M. (1995). Volcanic and structural evolution of Taupo Volcanic Zone, New Zealand: a review. *Journal of Volcanology and Geothermal Research* **68**, 1–28.

TABLES

1. General descriptions of each tephra unit in the Kohioawa and Ōtarawairere sections
2. Distinguishing characteristics of Kohioawa tephra types

APPENDICES

1. The characteristics of the magma types from Brown *et al.* (1998) using whole rock data from pumice clasts
2. Detailed descriptions of the horizons at the Kohioawa and Ōtarawairere sections
3. Major- and trace-element compositional means and 1-sigma uncertainties of glass data from clasts, including geothermometry and geobarometry modeling results
4. USGS RGM standard major element data

Table 1

Unit	**Thickness (KS; OS)**	**Samples (KS)**	**Samples (OS)**	**General Field Characteristics**	**Magma Type**	**Mineralogy (from field)**
Tablelands	55 cm; 170 cm	OK220707-1B	OK240707-1A	~3 horizons at both KS and OS; at OS, Tablelands sits atop a graywacke gravel base; layers vary from light cream/pink fine ash to orange-light brown fine and coarse ash; mostly fine-grained, fine-coarse ash, alternating layers with conspicuous biotite; the top of both sequences is finer grained, firm clay, with more sand at OS; the top of the sequence grades into a paleosol at OS and grades into paleosol at an adjacent outcrop at KS.	Tablelands+ Paerata	Plag Qtz Amph Bt
Paerata	150 cm; 205 cm	OK220707-1C; WHAK432A; WHAK432B; OK220707-1E; WHAK432C; OK220707-1F	Ōtarawairere-B	1 continuous horizon with subtle variations in grain size that define internal packages; the top and bottom of the package are dominated by fine-coarse ash; this unit is defined by the main package of the unit: yellow-orange, massive with subtle variations in grain size (coarse ash to fine lapilli), grain supported made up of mostly fine pumice lapilli, lithics, and crystals; there is a conspicuous 20 cm thick black organic paleosol at the top of the unit that grades into the main package at KS; sharp contact that varies in thickness at OS.	Tablelands+ Paerata	Plag Qtz Opx Amph Bt

Kohioawa	345 cm; 370 cm	OK220707-1G; WHAK432L; OK220707-1I; WHAK432D; WHAK432E; OK220707-1L; WHAK432F; OK220707-1N; WHAK432G; OK220707-1O	OK240707-1C; OK240707-1D; OK240707-1E; OK240707-1F	this unit is the thickest of all documented units in the Bay of Plenty (Manning 1995, 1996), and is subdivided into 3 main packages (dashed lines in Figure 2a); lowest Kohioawa package is predominantly massive and grain supported, with a finer horizon on top; Manning (1995) subdivided this lowest package into two subunits, as noted by a thin solid line in Figure 2a; at OS, base is grain supported, yellow-rust colored alternating layers of ash to fine-grained pumice lapilli; at KS, basal units are massive, grain supported fine-coarse ash and cream-light brown fine-coarse ash on top; middle Kohioawa package contains one horizon, which is the thickest horizon of the outcrops (~ 220 cm thick); subtle crossbeds in basal ~ 25 cm mark the beginning of this package; the rest of this horizon is massive and is coarser grained than the rest of the horizons in the outcrops; it is composed of predominantly ash sized to fine-lapilli sized juvenile clasts, crystals, and lava lithics; it is yellow, massive, and has fluctuations in grain size that define internal, grain supported packages of varying sized fine pumice lapilli; sharp contact with the upper horizons; top package is defined by thin horizons (~ 3 cm) of alternating coarse ash and grain-supported, very fine lapilli clasts with a light brown clay; these horizons then grade into a thick developed paleosol at KS which marks the top of this unit.	Kohioawa type A; Kohioawa type B; Kohioawa type C	Plag Qtz San Amph Opx Bt

Murupara-Bonisch	180 cm; 350 cm	OK220707-1P; OK220707-1Q; WHAK432H; WHAK432I; WHAK432J	OK240707-1J; OK240707-1L	alternating horizons between coarse and fine-grained material that becomes distinctly more friable and sandier than the rest of the outcrop; due to the cliff-like outcrop, observations and sampling are more difficult for this unit; at KS, ~8 thinner horizons, predominantly grain supported, cream to yellow to light brown, fine pumice lapilli to fine ashy alternating horizons, generally ~5-10 cm thick; several horizons fine upward; at OS, there are fewer defined horizons with thicker, fine ash; wavy bedding and alternating layers between thicker, finer grained layers; a paleosol separates the upper horizons at both locations; at KS, access with a ladder to the left of the main outcrop; upper layers are finer grained, ashy, less consolidated, and comprise a thick (>1 m), friable sandy ash deposit at the top of the outcrops; at KS, the Matahina ignimbrite overlies the Murupara-Bonisch unit.	Murupara-Bonisch type A; Murupara-Bonisch type B	Qtz Plag Amph Opx

Table 2

	Kohioawa type A	Kohioawa type B	Kohioawa type C
SiO_2	77.0-77.9	77.2-77.8	77.3-78.2
CaO	0.77-1.00	0.55-0.68	0.48-0.59
TiO_2	0.13-0.21	0.05-0.14	0.04-0.09
FeO	1.05-1.48	0.82-1.02	0.68-1.04
MgO	0.09-0.18	0.02-0.07	0.02-0.06
Sr	43.0-75.6	20.5-37.4	8.0-20.3
Ba	649-910	298-869	72-223
Mn	223-366	341-425	379-493
Eu	0.31-0.53	0.18-0.38	0.12-0.34
U	3.5-20.9	6.8-25.5	10.6-20.3
Pb	14.8-19.8	16.7-27.4	17.6-24.1
Cs	5.6-8.3	7.2-9.3	8.2-12.3
Zr	74.5-136	64.4-88.4	63.8-98.0
Yb	1.9-2.8	2.2-3.0	2.6-3.6
Y	15.1-22.2	19.0-26.0	21.8-30.4